Development of high-affinity peptide ligands for serum albumin toward biomedical applications

ナカーエイ, エルナズ

https://doi.org/10.15017/1931749

出版情報：Kyushu University, 2017, 博士（工学）, 課程博士
バージョン：
権利関係：

2018

Doctoral Thesis

Development of high-affinity peptide ligands for serum albumin toward biomedical applications

Graduate School of Systems Life Sciences

Kyushu University

2018

Elnaz Nakhaei

Abstract

Development of high-affinity peptide ligands for serum albumin toward biomedical applications

Elnaz Nakhaei
Doctor of Philosophy
Graduate School of System Life Sciences
Kyushu University
2018

Thanks to the particular molecular and biological characteristics that the human serum albumin (HSA) has, developing strategies to design HSA-based drugs have been extensively evolved. Whether conjugation of these drugs with HSA is through non-covalent, covalent or genetic engineering, the ultimate purpose is to enhance the pharmacokinetic profile of the compound. HSA is the major circulating protein in the blood which has a long half-life of about three weeks. HSA also has a great ability to carry various types of endogenous and exogenous compounds in the blood, including different drugs. Thereby, affecting their distribution, absorption, metabolism and excretion profile. In a vast variety of disorders such as tumor tissues and inflamed sites. On the other hand, among the therapeutic compounds, proteins and peptides are very promising due to their selectivity, efficacy, and safety. However, their rapid elimination by enzymatic degradation or renal clearance has hindered their usage. To address this issue and to utilize the benefits of HSA, development of a more general and simpler delivery system based on HSA is required. In this thesis, I approached this goal through two methods.

In chapter 2, I could successfully enhance the blood circulation ability of a small fluorescent probe by modification of a palmitoyl group on a folate-fluorophore conjugate in

mice model. The alkylated probe maintained its specificity for binding to folate receptors which are overexpressed in many cancer cell types. Meanwhile, it induced an extended blood circulation through non-covalent binding to mouse serum albumin, compared with the probe lacking the alkyl group. It is supposed that this modified alkyl group could make non-covalent binding to the hydrophobic pockets of albumin. As a result, retaining the fluorescent probe for an extended time in the blood and higher accumulation in the tumor region. This result can be promising for the development of small fluorescent probes in near-infrared imaging used in the intraoperative imaging.

In chapter 3, I reported a novel design of peptide-based ligand with a strong binding affinity to human serum albumin (HSA), which can be used as a tag to extend the blood circulation of the small size molecules. I designed these ligands with dual alkyl groups connected with a negatively charged spacer. By a competitive binding technique, it was found out that the designed dual alkylated peptides with the tuned and shorter spacer were able to specifically share the HSA's binding pockets 4 and 6 for fatty acids, with a significantly higher binding affinity than that of the single alkylated peptide. Additionally, Cy7 modified dual alkylated peptide showed higher retention in the mice blood circulation than that of a single alkylated peptide, suggesting higher binding affinity of the former type of peptide to mouse serum albumin. No crystal structure of mouse serum albumin has so far been reported. But based on amino acid sequential studies, essential residues for the binding of fatty acids are nearly entirely conserved among all species. Thus, we can expect a similar binding behavior from human serum albumin and mouse serum albumin.

The novel approaches and findings in this research, may provide new insights into the development of more straightforward methods to utilize the unique advantages of HSA. And in a broader sense, they can lead realizing of more efficient and cheaper medications for severe diseases.

Contents

CHAPTER 1 Introduction

The effectiveness of a drug is dependent on its bioavailability and sufficient accumulation in the target site. It is crucial to reach desired concentration of a diagnostic or therapeutic drug in systemic circulation for pharmaceutical response to be shown whilst minimizing its side effects [1-5]. However, a large group of diagnostic and therapeutic agents has low-molecular-weight, a size below the renal clearance threshold, causing them to suffer from short plasma circulatory time besides non-specific accumulation [6, 7]. In the case of peptide or protein therapeutics, they also suffer from the proteolytic degradation. The short terminal half-life of these small drugs results in the requirement for a frequent dosing to maintain the therapeutic effects. It means an increase in the burden of medical expense and pain for the patients. To improve the pharmacokinetics parameters of peptide drugs, including their absorption, biodistribution, metabolism, and elimination, there is an enormous ongoing effort to implement half-life extension strategies [8, 9]. Depending on the endogenous clearance mechanism, several strategies have been introduced to increase the circulatory half-life of therapeutic peptides or proteins. These strategies include increasing the hydrodynamic volume/molecular mass (PEGylation), modification of N- and C-terminus or utilizing the neonatal Fc receptor recycling [5, 10, 11]. Among these strategies, human serum albumin (HSA) has emerged as one of the most important drug carriers for therapeutic active drugs and peptides thanks to being the most abundant natural carrier protein in the serum whilst having a long blood half-life of about 19 days [12-15].

In the path to reach a more general, stable and simpler delivery system based on HSA, in this thesis, I approached this objective using two methods. In the second chapter, I used a palmitoyl modification on a folate-fluorophore conjugate that besides targeting ability to tumor cells overexpressing folate receptor, it could induce long blood circulation through non-covalent binding to mouse serum albumin [16]. In the third chapter, I introduced a dual alkylated peptide which showed a higher binding affinity to its control, single alkylated peptide, which finally resulted in a longer blood circulation time in mice [17].

1.1 Unique characteristics of HSA for being a natural drug carrier

1.1.1 Abundance and substance-carrier ability

HSA (66.5 kDa) is the most abundant multifunctional plasma protein in the human bloodstream and tissue fluids. It is synthesized in the liver, exported as a non-glycosylated protein, and is present in the blood around 35-50 g/L (0.6 mM), comprising 60-65 % of the total plasma protein in humans (Table 1.1). Despite many other proteins, HSA is exceptionally robust towards pH, temperature, and organic solvents and can be stored as a 5 or 20% solution for many years [19, 20]. HSA's abundance, makes it an essential factor for the determination of drugs pharmacokinetics behavior, such as volume of distribution, as it binds to different varieties of drugs [21, 22]. Among its important functions are being responsible for 80% of the colloid osmotic pressure of blood and the transportation of various endogenous and exogenous compounds. These compounds range from long-chain fatty acids, metals, bilirubin, amino acids, vitamins to range of bioactive small molecule drugs. Typically, HSA ligands are accommodated primarily to one of the two high- affinity sites with typical binding association constants in the range of 10^4–10^6 M^{-1} (Table 1.2) [23, 24].

Table 1.1. Major circulating proteins and their concentration in the human blood. Albumin is the most abundant circulating protein with a long half-life [18,25].

Protein	Concentration (g/l)	MW (kDa)	%	Half life (days)
Total protein	66–83		100	
Albumin	35–55	66	50–70	19
IgG	8–15	150	12–18	21
IgA	1–4	160		5
IgM	0.5–2.5	900		5
Transferrin	2.2–3.7	90	3–4	8
Fibrinogen	2–4	340	3–5	4
All others	~2–5		1–6	

Table 1.2. Some groups of endogenous substances that bind to albumin [23].

Compound	Association constant, K_a (M^{-1})	n	Reference
Long-chain fatty acids	(1-69) x 10^7	1	Richieri *et al.* (1993)
Eicosanoids (PGE_1)	7 x 10^4	2	Unger (1972)
Bile acids	(3-200) x 10^3	3	Roda *et al.* (1982)
Steroids			
Cortisol	5 x 10^3	2	Yates and Urquhart (1962)
Progesterone	3.6 x 10^5	1	Ramsey and Westphal (1978)
Testosterone	2.4 x 10^4	1	Pearlman and Crepy (1967)
Aldosterone	3.2 x 10^3	1	Richardson *et al.* (1977)
Bilirubin	9.5 x 10^7	1	Brodersen (1982)
Hematin	1.1 x 10^8	1	Adams and Berman (1980)
L-Thyroxine	1.6 x 10^6	1	Kragh-Hansen (1981)
L-Tryptophan	1.0 x 10^4	1	McMenamy and Oncley (1958)
25-OH-Vitamin D_3	6 x 10^5	1	Bikle *et al.* (1986)
1,25-$(OH)_2$-Vitamin D_3	5 x 10^4	1	Bikle *et al.* (1986)
Aquocobalamin	2 x 10^7	1	Lien and Wood (1972)
Folate	9 x 10^2		Soliman and Olesen (1976)
Ascorbate	3.5 x 10^4	0.1	Molloy and Wison (1980)
Copper(II)	1.5 x 10^{16}	1	Masuoka *et al.* (1993)
Zinc(II)	3.4 x 10^7	1	Masuoka *et al.* (1993)
Calcium	15.1 x 10^2	1	Kragh-Hansen and Vorum (1993)
	6.5 x 10^2	3	
Magnesium	1 x 10^2	12	Pedersen (1972)
Chloride	7.2 x 10^2	1	Scatchard and Yap (1964)
	6.1 x 10^1	4	

1.1.2 Long circulatory half-life

As it was mentioned in the introduction, HSA has a long blood half-life of about 19 days (Table 1.1) and the secret behind this uniquely long half-life is its salvage from lysosomal degradation by neonatal Fc receptor (FcRn) mediated recycling [26]. This major histocompatibility complex-related Fc receptor protects HSA and IgG, from catabolic degradation fate by binding both proteins with high affinity in a pH-dependent fashion only at a low pH (pH < 6.5) in acidic endosomes, preventing their degradation via the lysosomal pathway and returning them to the extracellular space (pH 7.4) [28]. HSA is taken up by pinocytosis nonspecifically along with IgG from the extracellular milieu to be transported to acidic endosomes. In these early endosomes, acidic milieu facilitates binding of HSA to FcRn.

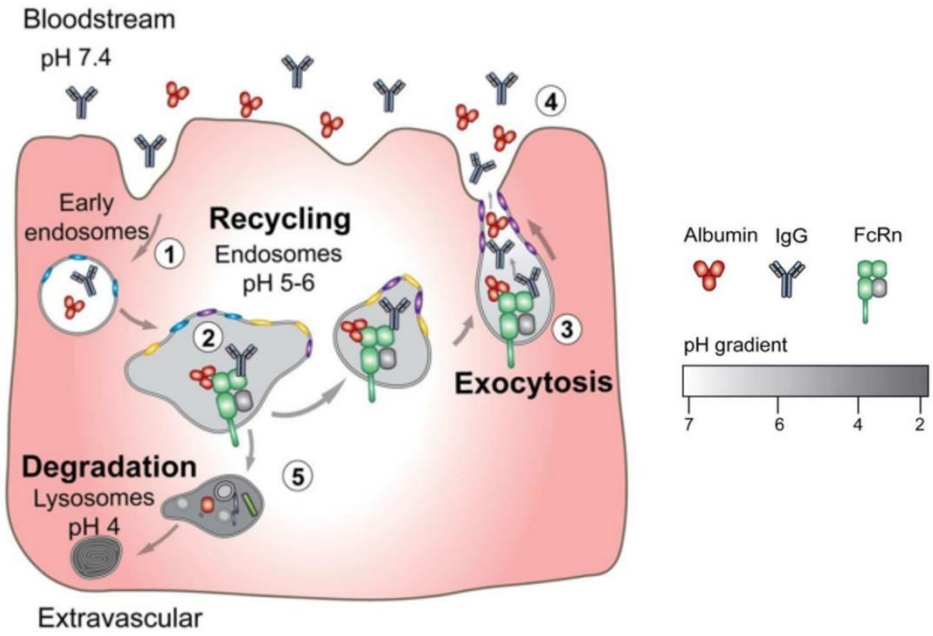

Figure 1.1. FcRn-mediated transport pathways. A schematic illustration of the model of FcRn-mediated recycling pathway of its two ligands in an endothelial cell lining the vascular space. (1) IgG and albumin are taken up from the blood by pinocytosis in early endosomes. (2) FcRn, predominantly localized to acidified endosomes, binds the ligands (3) The ternary complex is recycled to the cell surface as which results in exocytosis of the ligands. (4) The neutral pH of the bloodstream leads to release of the ligands. (5) Proteins that do not bind to the receptor will be sorted to late endosomes and further to lysosomes for degradation [27].

Therefore, HSA or any compound bound to it escapes the late endosome and the subsequent degradation in the lysosome. The complex is then recycled to the cell surface, where progressively reaching to the neutral pH triggers release of intact HSA out of the cell and back to the circulation [28, 29] (Figure 1.1).

This mechanism consequently extends the half-life of HSA. For desiging FcRn is widely distributed in many tissues and cell types including vascular endothelial cells, gut, antigen presenting cells, upper airway, renal, colorectal, mammary and brain endothelial cells. It has also been suggested that this albumin protection mechanism is widespread among animals from three species of human, rat and mouse [29]. Therefore, the unique ability of this receptor to prolong the half-life of albumin and its widespread existence in many cell types a have guided engineering of novel therapeutics [27, 30, 31].

1.1.3 High accumulation in tumor tissues and inflamed sites

Studies have demonstrated that albumin has a shorter half-life and a higher rate of accumulation in tumor-bearing mice, despite a compensatory increase in hepatic albumin synthesis, compared to non-tumor-bearing mice. Investigations have shown that tumors metabolize substantial amounts of albumin, using it as a source of nitrogen and energy. Therefore, it has been suggested that tumors utilize albumin as a source of energy, by breaking down albumin into its component amino acids that are subsequently used by cancer cells for their accelerated growth [25, 32]. Moreover, studies have suggested that the hypoalbuminemia evident in cancer patients is a result of albumin catabolism by the tumor. Due to lacking a functional lymphatic system and the leakiness of tumor vessels, the rate of albumin extravasation and its accumulation in tumor tissues are noticeably increased [33, 34]. The uptake of albumin in tumor cells itself occurs by fluid phase endocytosis followed by lysosomal breakdown [25, 35]. Therefore, HSA-based nanoparticles or tumor imaging agents can accumulate more efficiently in the tumor site by this effect of enhanced permeability and retention (EPR). The tumor-targeting properties of HSA-based nanoparticles is also attributed to the transcytosis mediated by albumin receptors such as the 60-kDa glycoprotein pg60, located on endothelial cell surface, which leads to increased drug transport directly into tumor cells [36]. Albumin binds to gp60 with a high binding affinity of nanomolar range and it is followed by transcytosis of both gp-60-bound and fluid phase albumin through the tumor endothelium into the subendothelial space. Upon entering the tumor interstitium, SPARC protein (Secreted Protein Acidic and Rich in Cysteine), a 43-kDa secreted matricellular glycoprotein with high binding affinity to albumin and significant homology to gp60 traps albumin [37, 38]. It is followed by lysosomal degradation inside the cell to provide the energy source for tumor proliferation. Thus, albumin-coupled drugs are released within the tumor cells [39]. Over-expression of SPARC as a critical modulator of extracellular matrix proliferation, and cell migration correlates with an increased tumor invasion, metastasis, and poor prognosis in multiple tumor types [40]. Therefore, targeting SPARC protein can enhance tumor targeting of albumin-binding nanoparticles [41].

Similar to tumor cells, HSA is also well-known as having a relatively high uptake in inflamed tissue. Under cellular stress-inducing conditions, cells preferentially take up HSA as the main energy source for growth and maintenance. In patients with rheumatoid arthritis, the permeability of the blood-joint barrier for albumin in markedly increased, and they frequently

develop hypoalbuminemia due to increased albumin turnover [42]. Therefore, by utilizing this high uptake of albumin in inflamed tissues and the long half-life of albumin, new conjugates of antiproliferative drugs like methotrexate to albumin has been developed, which results in lower dosage frequencies and side effects [34].

Due to high plasma concentration of HSA and its multifunctionality, e.g., serving as a transport protein for numerous compounds, HSA is closely-involved in an extensive variety of diseases. Besides cancer and inflammation, involvement of HSA in diseases such as amyloidotic polyneuropathy or Alzheimer's disease is well-documented as well [43]. Therefore, based on the molecular pathologies of such conditions, a variety of safe and novel HSA-based therapeutic strategies can be developed.

1.2 Structural and ligand-binding properties of HSA

1.2.1 Structure of HSA and drug binding sites

Human serum albumin can bind a remarkable variety of drugs impacting their delivery and efficacy and ultimately altering the distribution and the free, active concentration of many administrated drugs. HSA is a monomeric protein of 585 amino acids organized into three homologous helical domains (I-III), that assemble to form a heart-shaped molecule. Each domain is comprised of two subdomains (A and B); I (residues 1-195), II (196-383), and III (384-585), respectively (Figure 1.2). Each domain possesses common structural motifs. However, the whole protein is highly asymmetric in structure and binding properties. The principal regions of ligand binding to HSA are located in hydrophobic cavities in subdomains IIA and IIIA, which exhibit similar chemistry. Although helices are often considered to be rigid units of construction, the interdomain helices in HSA allow for considerable movement. This movement is particularly evident upon fatty acid binding but may also occur as part of albumin's breathing motion in solution. [44, 45].

The structure is stabilized by 17 disulphide bonds, which are all intra-subdomain and follow a nearly perfectly repeated pattern within each domain. These disulphide bonds are involved in locking together helices within the same sub-domain and it is believed that they contribute to the remarkable thermal stability of HSA [23, 44]. There is only one free, unpaired Cys located in the subdomain IA, which makes it a potentially important circulatory

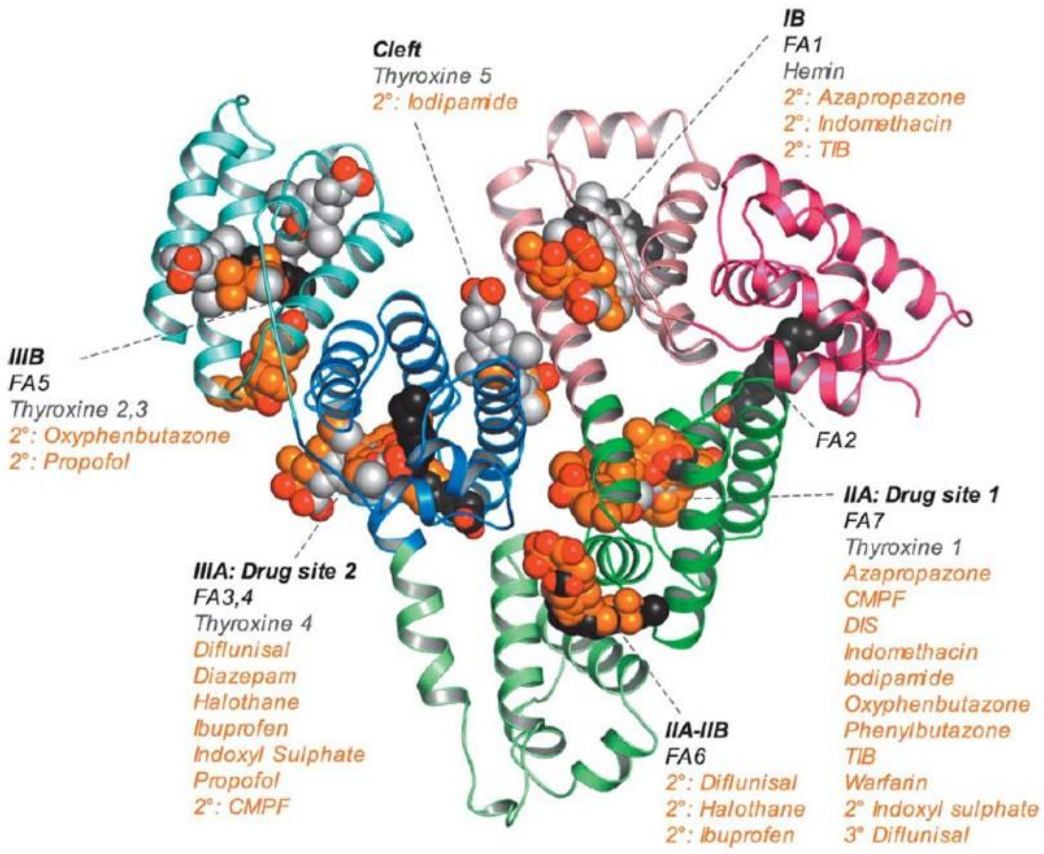

Figure 1.2. Summary of the ligand binding capacity of HSA as defined by crystallographic studies to date. Ligands are depicted in space-filling representation; oxygen atoms are colored red; all other atoms in fatty acids (myristic acid), other endogenous ligands (hemin, thyroxin) and drugs are colored dark-grey, light grey and orange, respectively. Warfarin, an anti-coagulant drug, and ibuprofen, a non-steroidal anti-inflammatory agent, are considered as stereotypical ligands for Sudlow's site I and Sudlow's site II, respectively [47].

antioxidant. This free thiol functional group in HSA has been exploited to develop in situ coupling of thiol-reactive prodrugs, such as acid-sensitive hydrazine derivative of doxorubicin [14, 46].

The structure explains numerous physical phenomena and should provide insight into future pharmacokinetic and genetically engineered therapeutic applications of serum albumin. HSA binds a great number of therapeutic drugs such as antibiotics, anticoagulants, anti-inflammatory drugs, anesthetics and benzodiazepines to name just a few. It acts as a detoxifying protein binding for bilirubin, the breakdown product of heme, and heavy metal ions such as lead(II) and platinum(II). Though diverse in structure, these ligands bind to albumin because it is selective for hydrophobic molecules that have electronegative or

negatively charged features [23]. It is well-documented that two primary, non-overlapping drug-binding sites exist on the domain IIA and IIIA of HSA. These two sites are referred to Sudlow's site I and II or drug site 1and site 2, respectively [48]. Bulky heterocyclic anions bind to drug site 1, whereas drug site 2 is preferred by aromatic carboxylates with an extended conformation (Figure 1.2). All of the compounds bound to drug site 1, are positioned to make a hydrogen bond interaction with the hydroxyl group of Y150, located in subdomain IIA. Drug site 2 is composed of all six helices of subdomain IIIA and is therefore topologically similar to site 1 (subdomain IIA). Drug site 2 is smaller than site 1, however, the entrance to site 2 is not obstructed, as it does in the site 1 entrance. Even though subdomain IIIA is followed by IIIB, this subdomain is rotated further away from the drug site entrance (in comparison to drug site 1, domain II) and leaves the pocket entrance more exposed to solvent [48], therefore more accessible for interaction with hydrophobic compounds. The interior of the binding pocket in site 2 is hydrophobic, with a single polar patch near to the entrance centered on Arg410 and Tyr411 but also including Lys414 and Ser489. In spite of its relative rigidity, site 2 also possesses a degree of conformational adaptability by its capacity to bind two molecules of long-chain fatty acids simultaneously [49].

In short, the binding specificities of the pockets are determined by their shapes and the particular distributions of basic and polar residues on the largely hydrophobic interior walls that are involved in charge neutralization and hydrogen bonding interactions with acidic or electronegative small molecule ligands [47].

1.2.2 Fatty acid binding

HSA is also the primary binding protein in the trafficking of fatty acids and is able to bind fatty acids (FAs) at multiple binding sites with different affinities. The structure of HSA in complex with medium and long-chain saturated fatty acids (C10, C12, C16 and C18) have been reported [50]. For these fatty acids seven common binding sites have been identified, distributed across the protein [50]. These seven common sites exhibit substantial structural differences from one another despite the repeating domain structure of the protein (Figure 1.3). The fatty acid sites are variously contained entirely within one subdomain (site 1, 4, 5 and 7), at a domain interface (site 2 and 3), or at the interface between two subdomains belonging to the same domain (site 6).

In sites FA1-5 the carboxylate moiety of fatty acids is anchored by electrostatic/polar interactions [51]. FA5 is located within subdomain IIIB with the polar head orientated towards subdomain IIIA and establishes both salt bridges and hydrogen bond with Tyr401 and Lys525. On the contrary, sites FA6 and FA7 do not display a clear evidence of polar interactions that keep in place the carboxylate head of the fatty acid, thus suggesting that sites FA6 and FA7 are low-affinity FA binding sites [51, 52]. Under physiological conditions, HSA normally binds up to two moles of unesterified fatty acids, although it may accommodate up to six moles under certain disease states [53]. It is considered that most reactive species toward albumin is carboxyl group which is agreement with the drugs and endogenous substances that contain –

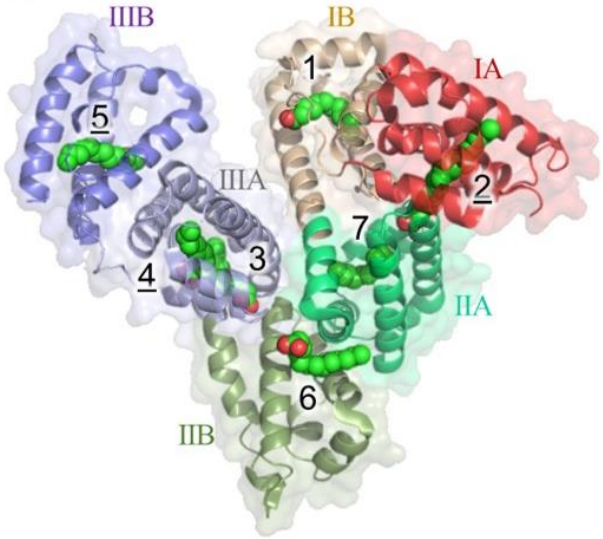

Figure 1.3. Crystal structure of myristic acid bound to HSA (PBD: 1E7G). Seven binding sites for fatty acid ligands are described in black digits. Pocket number with underbar are strong binding pockets for hydrophobic compounds.

COOH groups [48, 54]. In essence the three domains are each adapted differently for fatty acid binding and no two binding sites are alike in detail, although each comprises a hydrophobic pocket capped at one end with basic or polar side chains. [55].

1.3 HSA-based drug delivery

As described previously, HSA has particular features such as, having a size above the renal filtration threshold, being able to escapes the lysosomal degradation by FcRn recycling while it is involved in many disorders. In order to employ these advantages, various molecules have been joined to albumin either non-covalently (specific binding to albumin) or covalently (conjugation and direct genetic fusion) to improve their pharmacokinetic profile [15]. In Table 1.3. Some of small therapeutic molecules are summarized based on their method of attachment to albumin, along with their calculated circulatory half-time improvement from the animal model system.

Non-covalent binding of an insulin detemir (Levemir®) binds to HSA after its slow diffusion into the injection site and entering to the systemic circulation, significantly has prolonged its half-life [14, 57, 58]. The former is an insulin analog in which a fatty acid (myristic acid, C14) is bound to the recombinant lysine amino acid at insulin position B29. However, binding affinity of this insulin detemir had been determined as 2.4×10^5 M^{-1}, which is at least one magnitude lower than that of the free myristic acid [57, 58]. The ability of albumin to bind endogenous ligands such as fatty acids had been also exploited in the development of glucagon-like-1 peptide derivative (Victoza®, Table 1.4) with a myristoyl at its ε-amino position of the N-terminal lysine. Victoza® is also administrated for the treatment of diabetes and obesity [59, 60].

HSA also had been utilized to overcome the solubility problem of some highly hydrophobic drugs such as anticancer paclitaxel [61]. Albumin-bound paclitaxel (Abraxane®), is prepared by mixing the drug with HSA in an aqueous solution, and passing the mixture through a high-pressure homogenizer to form drug-loaded albumin nanoparticles. This nanoparticle shows much lower side effects, higher tolerance of higher drug dosage with a more efficient accumulation in tumor sites utilizing the gp60 receptor of albumin [38, 62].

Albumin has been extensively explored for improvement of the pharmacokinetic and blood circulation time of many antibodies and therapeutic peptide [5], as they exhibit short

plasma half-lives due to e.g. proteolytic elimination [6]. Albumin-binding domain bound to antibodies or albumin fusion antibody are profoundly explored methods to utilize the long circulation ability of HSA [63, 64]. For this purpose, it is of great importance to consider the complex structure of FcRn with HSA and avoid modification or hindering the FcRn binding region of HSA (Figure 1.4). The main areas of application for exploring albumin-based drugs are diabetes, oncology, rheumatology, vascular and imaging. Table 1.4 shows an overview on some ongoing clinical trials or approved albumin-based drug delivery systems [14, 15].

Table 1.3. Improvement of the pharmacokinetic profile of various molecules joined to albumin using different modes of interaction [15].

Mode of interaction with albumin	Active pharmaceutical ingredient	PK model	Terminal half-life without albumin PK enhancement	Terminal half-life with albumin PK enhancement	Terminal half-life improvement factor	Clinical status
Non-covalent binding	Insulin detemir	Human	4–6 min	5–7 h	50–105	Approved
	GLP-1	Human	1.5–2 min	11–15 h	330–600	Approved
	scFv	Mouse	20 min	40 h	120	Preclinical
	IFNα-2b	Mouse	1.2 h	22.6 h	19	Preclinical
	Fab	Rabbit	0.8 h	32.4 h	40.5	Preclinical
		Mouse	0.4 h	10.4 h	26	
	Anti-EGFR	Mouse	1 h	44 h	44	Preclinical
	IL-1RA	Mouse	2 min	4.3 h	129	Preclinical
	G-CSF	Rat	2.1 h	23.7 h	11.3	Preclinical
	IFNα-2b	Rat	1.2 h	22.6 h	18.8	Preclinical
Covalent attachment	GLP-1	Human	1.5–2 min	9–15 days	6480–14,400	Phase I completed
	Exendin-4	Human	<1 h	8 days	192	2 Phase II studies completed, a 3rd Phase II terminated[1]
	Doxorobicin					Phase I completed
	Methotrexate					Phase II
Genetic fusion	GLP-1	Human	1.5–2 min	5 days	3600–7200	BLA submitted
		Cynomolgus monkey	1.5–2 min	2–4 days	1440–5760[2]	
		Mouse	1.5–2 min	11 h	330–660[2]	
	G-CSF	Human	2.5 h	18–40 h	7.2–16	Phase III completed
		Cynomolgus monkey	2.5 h	7–13 h	2.8–5.2[3]	
		Mouse	2.5 h	6 h	2.4[3]	
	FVIIa	Rat	39.5–45.6 min	262.7 min	5.8–6.7	Phase I completed
	FIX	Human	17.1 h	92 h	5.4	Phase III initiated
		Cynomolgus monkey	12.7 h	39.8 h	3.1	
		Dog	23.5 h	55.2 h	2.3	
		Rabbit	9.1 h	29.6–36.2 h	3.3–4	
		Rat	5.1 h	17.4–24.1 h	3.4–4.7	
	scFv	Rat	3.5 h	27.7–30.8 h	7.9–8.8	Preclinical
	IFNα-2b	Human	2–3 h	140–159 h	47–80	Phase III completed, BLA withdrawn
		Cynomolgus monkey	5 h	90 h	18	
		Rat	1.2 h	14.2 h	11.8	
Micro-/Nanoparticle	Paclitaxel					Marketed
	Technetium-99					Marketed
	Docetaxel					Phase I/II

[1] Commercial decision.
[2] The terminal half-life improvement factor is calculated relative to GLP-1 in human.
[3] The terminal half-life improvement factor is calculated relative to G-CSF in human.

Considering the high selectiveness and efficacious of peptides and, at the same time their safety, there is an increased interest in development of therapeutic peptides. Despite this potency, peptide' clinical use is still limited due to the insufficient delivery and systemic stability. Also, no generalizable strategy for the delivery of peptide therapeutics has been found [10, 65]. That being said, designing of more general molecular strategies that can take advantage of HSA binding properties may lead in improve the pharmacokinetic profile of higher number of potential peptide.

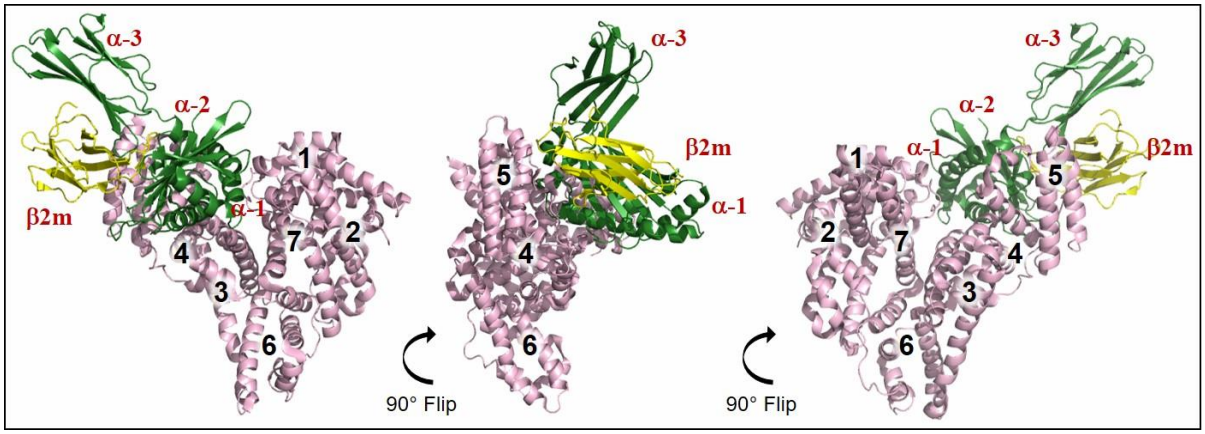

Figure 1.4. Human FcRn complexed with HSA (PDB: 4N0F). The figure was designed using PyMol software. FcRn, recycling receptor of HSA, is a major histocompatibility complex (MHC) class I. FcRn's extracellular domains are described in red (α1, α2, α3 and β2m). Seven binding sites for fatty acid ligands are described in black digits.

Table 1.4. Overview of albumin-based drugs that have reached market approval or are in different stages of clinical development [2, 15].

Indication	Phase I	Phase II	Market Approval
Diabetes			**Levemir®** A myristic acid derivative of insulin **Victoza®**A myristic acid derivative of GLP-1
Diabetes		**CJC-1134-PC** [60] An albumin conjugate of GLP-1	
Oncology - Breast cancer - Pancreatic cancer - Lung cancer			**Abraxane®** An albumin nanoparticle of paclitaxel
Oncology - Soft tissue sarcoma - Pancreaticcancer		**INNO-206** [66] An albumin-binding prodrug of doxorubicin	
Oncology - Breast cancer	**MM-111** [63] An albumin fusion protein incorporating two scFv directed against Erb2 and Erb3		
Oncology - Glioblastoma, diagnostic tool for surgery		**AFL-HAS** [67] A fluorescein-labeled albumin conjugate	
Oncology - *In vivo* imaging of HER-2-expressing tumors	**ZHER2:342** [64] An affibody molecule for binding to the HER2 receptor		
Rheumatoid Arthritis		**ATN-103** [68] An albumin-binding trivalent nanobody directed against TNF-α	
Oncology Rheumatology			**Nanocoll®,** [69] **Albures®** [70] ^{99m}Tc-aggregated albumin for diagnostic use in nuclear medicine
Vascular disease - MRI contrast agent			**Vasovist®** [71] An albumin-binding Gadolinium(III) complex

1.4 Overview of this thesis

In the path to reach a more general, stable and simpler HSA-based delivery of small therapeutic compounds, I used two types of approaches.

In the first approach, I tried to enhance the blood circulation ability of a small fluorescent probe by modification of a palmitoyl group on a folate-fluorophore conjugate. This single alkylated probe, could maintain its show specificity for binding to folate receptors which are overexpressed on many cancer cell types. Meanwhile, it induced long blood circulation through non-covalent binding to mouse serum albumin. This result can be promising for development of small fluorescent probes in near-infrared imaging used in the intraoperative imaging.

In the second approach, mainly I investigated the modification of two alkyl chains on a peptide ligand and its effect on binding affinity to the HSA. The peptide itself was designed negatively-charged so it can make electrostatic interaction with the basic-capped pockets of HSA. I found out that the dual alkylated peptides showed higher binding affinities to HSA compared to their control, single alkylated peptide. Eventually, I could observe the impact of this dual alkylation *in vivo*, in which dual alkylated peptide resulted in a longer blood circulation time in mice compared with that of the single alkylated peptide.

Thereby, finding new and straightforward methods to utilize the unique advantages of HSA can be promising to realize more efficient and cheaper medications for severe diseases.

1.5 References

[1] S. C. Penchala, M. R. Miller, A. Pal, J. Dong, N. R. Madadi, J. Xie, H. Joo, J. Tsai, P. Batoon, V. Samoshin, A. Franz, T. Cox, J. Miles, W. K. Chan, M. S. Park and M. M. Alhamadsheh, *Nat. Chem. Biol.*, 2015, **11**, 793–798.

[2] F. Kratz and B. Elsadek, *J. Control. Release*, 2012, **161**, 429–445.

[3] V. Torchilin, *Adv. Drug Deliv. Rev.*, 2011, **63**, 131–135. M. T. Larsen, M. Kuhlmann, M. L. Hvam and K. A. Howard, *Mol. Cell. Ther.*, 2016, 1–12.

[5] M. Werle and A. Bernkop-Schnürch, *Amino Acids*, 2006, **30**, 351–367.

[6] N. Bertrand and J. C. Leroux, *J. Control. Release*, 2012, **161**, 152–163.

[7] D. P. McGregor, *Curr. Opin. Pharmacol.*, 2008, **8**, 616–619.

[8] Z. Antosova, M. Mackova, V. Kral and T. Macek, *Trends Biotechnol.*, 2009, **27**, 628–635.

[9] R. E. Kontermann, *Curr. Opin. Biotechnol.*, 2011, **22**, 868–876.

[10] B. J. Bruno, G. D. Miller and C. S. Lim, *Ther. Deliv.*, 2014, **4**, 1443–1467.

[11] Andersen, J. T.; Sandlie, I. *Drug Metab. Pharmacokinet.* **2009**, *24* (4), 318.

[12] A. Hahnenkamp, W. Alsibai, C. Bremer and C. Höltke, *J. Control. Release*, 2014, **186**, 32–40.

[13] K. Chen, J. Xie and X. Chen, *Mol. Imaging*, 2009, **8**, 65–73.

[14] B. Elsadek and F. Kratz, *J. Control. Release*, 2012, **157**, 4–28.

[15] Sleep, J. Cameron and L. R. Evans, *Biochim. Biophys. Acta*, 2013, **1830**, 5526–5534.

[16] E. Nakhaei, C. W. Kim, D. Funamoto, H. Sato, Y. Nakamura, A. Kishimura, T. Mori and Y. Katayama, *MedChemComm*, 2017, **8**, 1190-1195

[17] E. Nakhaei, K. Takehara, H. Sato, K. Zai, A. Kishimura, T. Mori and Y. Katayama, Anal. Sci., in press.

[18] C. Lentner, Geigy scientific tables. / Volume 3, Physical chemistry, composition of blood, hematology, somatometric data, Ciba-Geigy International Medical and Pharmaceutical Information, Basle, 1984

[19] B. Farruggia and G. A. Picó, *Int. J. Biol. Macromol.*, 1999, **26**, 317–323.

[20] F. Kratz, *J. Control. Release*, 2008, **132**, 171–183.

[21] D. E. Epps, T. J. Raub and F. J. Kezdy, *Anal Biochem*, 1995, **227**, 342–350.

[22] F. Yang, Y. Zhang and H. Liang, *Int. J. Mol. Sci.*, 2014, **15**, 3580–3595.

[23] T. Peters Jr., All About Albumin, Academic Press Inc., USA, 1995.

[24] G. J. Quinlan, G. S. Martin and T. W. Evans, *Hepatology*, 2005, **41**, 1211–1219.

[25] G. Stehle, H. Sinn, A. Wunder, H. H. Schrenk, J. C. M. Stewart, G. Hartung, W. Maier-Borst and D. L. Heene, *Crit. Rev. Oncol. Hematol.*, 1997, **26**, 77–100.

[26] P. Prabhat, Z. Gan, J. Chao, S. Ram, C. Vaccaro, S. Gibbons, R. J. Ober and E. S. Ward, *Proc. Natl. Acad. Sci.*, 2007, **104**, 5889–5894.

[27] K. M. Knudsen Sand, M. Bern, J. Nilsen, H. T. Noordzij, I. Sandlie and J. T. Andersen, *Front. Immunol.*, 2015, **6**, 1–21.

[28] J. T. Andersen, J. D. Qian and I. Sandlie, *Eur. J. Immunol.*, 2006, **36**, 3044–3051.

[29] C. Chaudhury, S. Mehnaz, J. M. Robinson, W. L. Hayton, D. K. Pearl, D. C. Roopenian and C. L. Anderson, *J. Exp. Med.*, 2003, **197**, 315–322.

[30] C. L. Anderson, C. Chaudhury, J. Kim, C. L. Bronson, M. A. Wani and S. Mohanty, *Trends Immunol.*, 2006, **27**, 343–348.

[31] T. T. Kuo, K. Baker, M. Yoshida, S. W. Qiao, V. G. Aveson, W. I. Lencer and R. S. Blumberg, *J. Clin. Immunol.*, 2010, **30**, 777–789.

[32] J. Hradec, *Br. J. Cancer*, 1958, **12**, 290–304.

[33] R. K. Jain, *Cancer Res.*, 1988, **3890**, 2641–2658.

[34] A. Wunder, U. Muller-Ladner, E. H. Stelzer, J. Funk, E. Neumann, G. Stehle, T. Pap, H. Sinn, S. Gay and C. Fiehn, *J Immunol*, 2003, **170**, 4793–4801.

[35] J. R. Levick, *Arthritis Rheum.*, 1981, **24**, 1550–1560.

[36] J. E. Schnitzer, *Am. J. Physiol. Circ.*, 1992, **262**, 246–254.

[37] O. L. Podhajcer, L. G. Benedetti, M. R. Girotti, F. Prada, E. Salvatierra and A. S. Llera, *Cancer Metastasis Rev.*, 2008, **27**, 691–705.

[38] M. J. Hawkins, P. Soon-Shiong and N. Desai, *Adv. Drug Deliv. Rev.*, 2008, **60**, 876–885.

[39] C. Andersson, B. M. Iresjö and K. Lundholm, *J. Surg. Res.*, 1991, **50**, 156–162.

[40] C. S. Wang, K. H. Lin, S. L. Chen, Y. F. Chan and S. Hsueh, *Br. J. Cancer*, 2004, **91**, 1924–1930.

[41] B. Haley and E. Frenkel, *Urol. Oncol. Semin. Orig. Investig.*, 2008, **26**, 57–64.

[42] F. C. Ballantyne, A. Fleck and W. C. Dick, *Ann. Rheum. Dis.*, 1971, **30**, 265–70.

[43] M. Otagiri, Human serum albumin : new insights on its structural dynamics, functional impacts and pharmaceutical applications, *Sojo University Publishing Center*, Kumamoto, 2013

[44] Curry, S. *Funct. Impacts Pharm. Appl.* **2011**, *2011*, 1.

[45] S. Curry, H. Mandelkow, P. Brick and N. Franks, *Nat. Struct. Biol.*, 1998, **5**, 827–835.

[46] G. Candiano, A. Petretto, M. Bruschi, L. Santucci, V. Dimuccio, M. Prunotto, R. Gusmano, A. Urbani, and G. M. Ghiggeri, *J. Proteomics*, **2009**, *73*, 188.

[47] J. Ghuman, P. A. Zunszain, I. Petitpas, A. A. Bhattacharya, M. Otagiri and S. Curry, *J. Mol. Biol.*, 2005, **353**, 38–52.

[48] X. M. He and D. C. Carter, *Nature*, 1992, **358**, 209–215.

[49] F. Zsila, Z. Bikadi, D. Malik, P. Hari, I. Pechan, A. Berces and E. Hazai,

Bioinformatics, 2011, **27**, 1806–1813.

[50] A. A. Bhattacharya, T. Grüne and S. Curry, *J. Mol. Biol.*, 2000, **303**, 721–732.

[51] M. Fasano, S. Curry, E. Terreno, M. Galliano, G. Fanali, P. Narciso, S. Notari and P. Ascenzi, *IUBMB Life*, 2005, **57**, 787–96.

[52] J. R. Simard, P. A. Zunszain, J. A. Hamilton and S. Curry, *J. Mol. Biol.*, 2006, **361**, 336–351.

[53] D. P. Cistola and D. M. Small, *J. Clin. Invest.*, 1991, **87**, 1431–1441.

[54] Z. J. Yasseen, *J. Biomed. Sci.*, 2016, **5**, 1–8.

[55] S. Curry, P. Brick and N. P. Franks, 1999, **1441**, 131–140.

[56] S. Havelund, A. Plum, U. Ribel, I. Jonassen, A. Vølund, J. Markussen and P. Kurtzhals, *Pharm. Res.*, 2004, **21**, 1498–1504.

[57] P. Kurtzhals, S. Havelund, I. Jonassen, B. Kiehr, U. D. Larsen, U. Ribel and J. Markussen, *Biochem. J.*, 1995, **312**, 725–731. A

[58] Y. Fang, G. C. Tong and G. E. Means, *Biochim. Biophys. Acta*, 2006, **1764**, 285–91.

[59] C. R. Neumiller J, Sonnett T, Wood L, Setter S, *Diabetes, Metab. Syndr. Obes. targets Ther.*, 2010, **3**, 215–226.

[60] L. L. Baggio, Q. Huang, X. Cao and D. J. Drucker, *Gastroenterology*, 2008, **134**, 1137–1147.

[61] K. Paal, J. Muller and L. Hegedus, *Eur. J. Biochem.*, 2001, **268**, 2187–2191.

[62] R. Palumbo, F. Sottotetti, G. Trifirò, A. Ferzi, A. Gambaro, E. G. Spinapolice, E. Pozzi, B. Tagliaferri, C. Teragni and A. Bernardo, *Drug Des. Devel. Ther.*, 2015, **9**, 2189–2199.

[63] C. F. Mcdonagh, A. Huhalov, B. D. Harms, S. Adams, V. Paragas, S. Oyama, B. Zhang, L. Luus, R. Overland, S. Nguyen, J. Gu, N. Kohli, M. Wallace, M. J. Feldhaus, A. J. Kudla, B. Schoeberl and U. B. Nielsen, *Ther. Discov.*, 2012, **11**, 582–594.

[64] V. Tolmachev, A. Orlova, R. Pehrson, J. Galli, B. Baastrup, K. Andersson, M. Sandström, D. Rosik, J. Carlsson, H. Lundqvist, A. Wennborg and F. Y. Nilsson, *Cancer Res.*, 2007, **67**, 2773–2782.

[65] K. Fosgerau and T. Hoffmann, *Drug Discov. Today*, 2015, **20**, 122–128.

[66] R. Graeser, N. Esser, H. Unger, I. Fichtner, A. Zhu, C. Unger and F. Kratz, *Invest. New Drugs*, 2010, **28**, 14–19.

[67] R. Ding, E. Frei, M. Fardanesh, H. H. Schrenk, P. Kremer and W. E. Haefeli, *J. Clin. Pharmacol.*, 2011, **51**, 672–678.

[68] K. Coppieters, T. Dreier, K. Silence, H. De Haard, M. Lauwereys, P. Casteels, E. Beirnaert, H. Jonckheere, C. Van De Wiele, L. Staelens, J. Hostens, H. Revets, E. Remaut, D. Elewaut and P. Rottiers, *Arthritis Rheum.*, 2006, **54**, 1856–1866.

[69] K. Palosaari, J. Vuotila, R. Takalo, A. Jartti, R. Niemelä, M. Haapea, I. Soini, O. Tervonen and M. Hakala, *Rheumatology*, 2004, **43**, 1364–1373.

[70] Y.-F. Wang, M.-H. Chuang, J.-S. Chiu, T.-M. Cham and M.-I. Chung, *Tohoku J. Exp. Med.*, 2007, **211**, 379–385.

[71] R. B. Lauffer, D. J. Parmelee, S. U. Dunham, H. S. Ouellet, R. P. Dolan, S. Witte, T. J. McMurry, and R. C. Walovitch, *Radiology*, 1998, **207**, 529-538.

CHAPTER 2

Design of a ligand for cancer imaging with long blood circulation and enhanced accumulation ability in tumors

2.1 Introduction

Tumor imaging has become an important technology in cancer diagnostics and prognosis. Many types of imaging molecular probe for various modalities, such as positron emitting tomography (PET), magnetic resonance imaging (MRI), and computed tomography (CT) have been successfully introduced into clinical practice [1, 2]. Intra-operative diagnosis is another promising technique to visualize tumor regions in tissue. This technique should improve the efficiency of removal of tumor tissues during surgery, as it assists real-time feedback in monitoring residual malignant tissues, thus contributing to improved overall survival [3-5].

In the development of intra-operative imaging techniques, fluorescence detection is one of the most promising modalities due to its high sensitivity and resolution. However, a fluorescence probe for intra-operative use has not been fully developed. The molecular probes should have some essential characteristics, such as high specificity against target cancer cells and sufficient accumulation and retention in the tumor tissue.

To ensure cancer specificity, tumor cell-specific targeting ligands are usually used [5-7]. Thus, certain receptors, such as glutamine transporter, EGFR or folate receptor, that are overexpressed in various cancer cells have emerged as optimal targets for imaging (Figure 2.1) [8-11]. However, imaging probes using targeting ligands are in general rapidly excreted from kidneys during systemic application due to their small size [3, 8, 12, 13]. This results in a demand for a higher dose of the probe and limited intraoperative surgery, as the surgery requires several hours. Thus, the size of the probe may be one of the critical factors for long circulation in the blood. Probes smaller than 5 nm are easily excreted through renal clearance, while probes larger than 500 nm are captured by liver and spleen [13, 14]. Therefore, fluorescence imaging probes should range in size between 5 to 500 nm. The size of probe is also a key point for its specific accumulation and retention in the tumor. In normal tissues, well-organized blood vessels have regular and integrated structure. However, in tumor tissues, the neovasculature enhances extravasation of macromolecules that are smaller than 100 nm, and incomplete lymph duct also contributes to the retention of such macromolecules in tumor

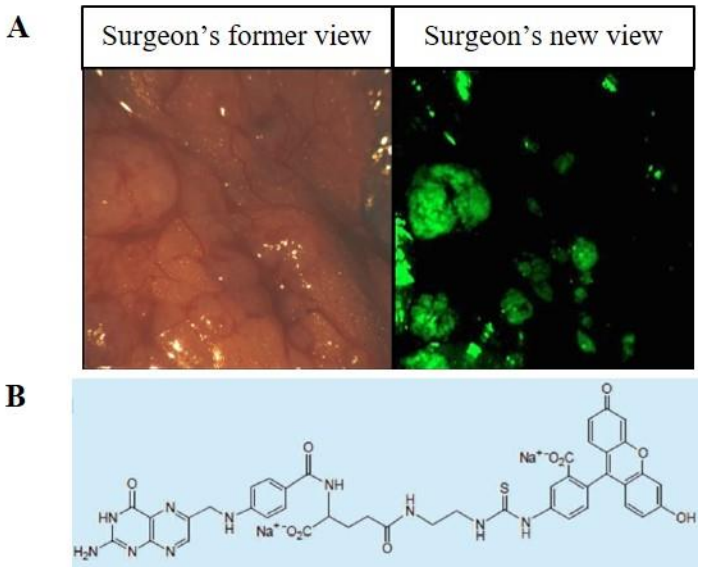

Figure 2.1. (A). View of localized region in peritoneal cavity of an ovarian cancer patient as seen with the aid of a folate-FITC conjugate (B).

tissue. This effect is known as the enhanced permeability and retention effect and has been used in many types of tumor delivery methods as a gold standard [15, 16]. However, from the practical viewpoint, such probes may have some drawbacks, such as difficulty with production and regulation of its characteristics.

This study focused on the improvement of the circulation ability and accumulation of a targeted fluorescent molecular probe for tumor imaging by using a small molecule. Human serum albumin (HSA; 66.5 kDa) is the most abundant plasma protein in the blood (ca. 0.6 mM, ~ 42 g/L) and tissue fluids, with an average half-life of 19 days in blood circulation; HSA can also strongly bind various small molecules [17, 18]. This binding property of HSA has resulted in research efforts to design and develop drugs with high binding affinity against HSA to either improve the pharmacokinetics profile or bioavailability of drugs [19-21]. HSA also shows relatively high uptake in tumor and inflamed tissues [22, 23]. Under cellular stress-inducing conditions, such as fast-growing tumors, cells preferentially take up HSA as the main energy source for growth and maintenance [24].

Considering these features of HSA, it was hypothesized that long blood circulation time and effective accumulation and retention in cancer would be rendered to a small fluorescence probe molecule that could bind HSA [25-28]. A long alkyl chain, which is a good ligand for HSA, was incorporated into a tumor-specific fluorescence small molecule. The probe also contains a folate (folic acid, FA) derivative to secure tumor specificity. Among the targeting

ligands folate (folic acid) targeted drug delivery has emerged as a highly selective tumor marker for the treatment and imaging of many cancers and inflammatory [9-11]. The expression of folate receptors is largely restricted to cells important for embryonic development and folate resorption (kidney) and is overexpressed in greater than 90% of ovarian carcinomas, as folate is needed in the synthesis of nucleotide bases. Among the three FR isoforms, FRα is the most widely expressed, with very low levels in normal tissues, but high expression levels in many tumors, though with a wide range [9, 29]. FRα has a dissociation constant (K_d) for folate of ~ 0.1 nM, which is approximately 10-fold lower than its K_d. for reduced folates which are the substrate for normal cells. As such, FRα has become the molecular target for the development of many cancer targeting compounds [10-12]. The structure of FRα contains a long and open folate binding pocket, which is formed by the amino-terminal loop. Folate is oriented with its basic pteroate moiety docked deep inside of the negatively charged pocket and the two negatively charged carboxyl groups of its glutamate moiety solvent-exposed sticking out of the positively charged entrance of the ligand-binding pocket (Figure 2.2). The interactions around the pteroate moiety contain both hydrogen bonds and hydrophobic interactions [30]. Based on these characteristics I decided to design and evaluate the fluorescent imaging probe by applying targeting the folate receptor system.

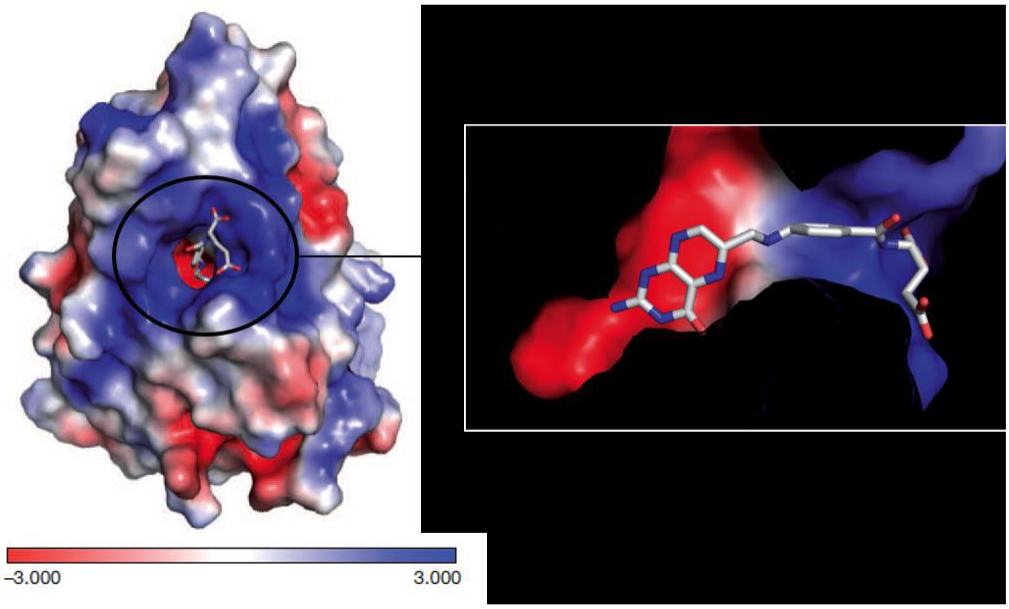

Figure 2.2. Structure of folate receptor α (FRα) bound to folate, with a close-up view of ligand bindinig positively charged pocket entrance. Folate carbon atoms are coloured grey, nitrogen atoms blue, and oxygen atoms red. A colour-code bar (bottom) shows an electrostatic scale from -3 to +3 eV.

2.2 Results and discussion

2.2.1 Design and synthesis of the fluorescence probe interacting with HSA for cancer imaging

Structures of the synthesized probes are shown in Figure 2.3. It was hypothesized that introduction of a natural ligand for HSA to a fluorescence probe molecule would result in an enhancement of blood circulation ability from the reversible interaction with HSA. This may be advantageous for *in vivo* stability compared with covalent bonding of the probe to HSA due to the lack of any denaturation or introduction of a non-natural structure, which may be recognized by the immune system. The C-terminus of the probe was modified with a palmitoyl group. Palmitic acid is naturally carried by HSA in the blood circulation with a strong affinity [31]. For tumor targeting, I used the folate moiety, as various cancers show overexpression of folate receptor. Between the folate moiety and the palmitoyl group, hydrophilic oligo-ethylene glycol was also incorporated to increase solubility and help the binding of the folate moiety with its receptor on cancer cells. The molecule was successfully synthesized by solid phase synthesis with standard Fmoc chemistry.

For *in vivo* assays, the amine-reactive succinimide ester of Cy7 was incorporated in the probe. Cy7 has a high quantum yield of 20% and high photostability and is especially useful for near infra-red (NIR) imaging. NIR Cy7 fluorescent imaging takes advantage of the transparency of biological tissues with the maximum excitation wavelength of 740 nm and a maximum emission wavelength of 773 nm. The obtained probe **2** and the control probe **3** were identified by MALDI-TOF-MS (Figure 2.4). I synthesized the Rhodamine-conjugated probe (probe **1**) for the *in vitro* experiments in the same manner.

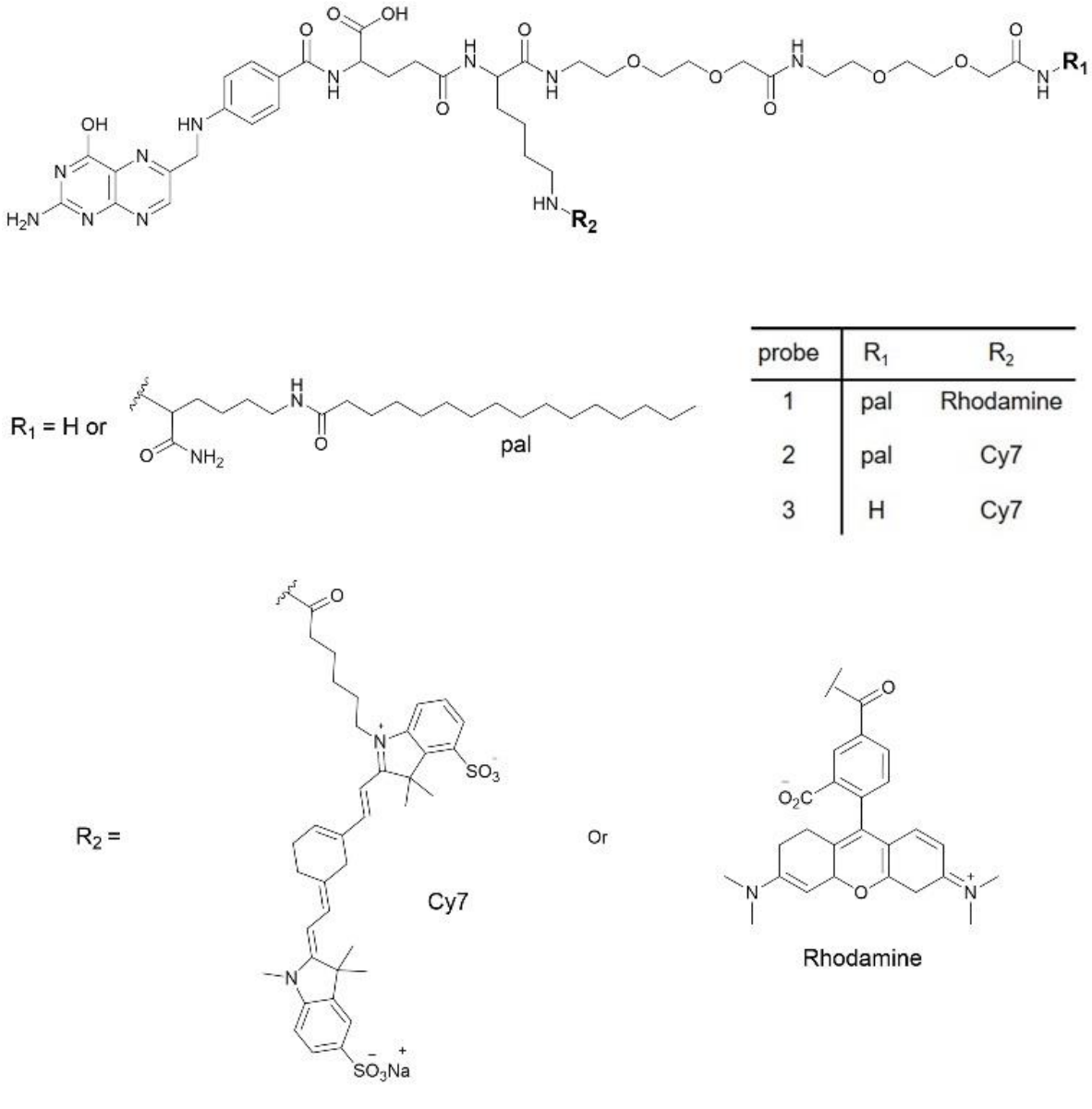

probe	R_1	R_2
1	pal	Rhodamine
2	pal	Cy7
3	H	Cy7

Figure 2.3. Chemical structure of the synthesized fluorescent probes 1, 2 and 3. The R_1 and R_2 substituents in each probe are described in the inset table. Probe 1 was used in in vitro experiments and probes 2 and 3 were used in *in vivo* experiments. To introduce. To introduce the palmitoyl group (pal) on the probe, the probe was modified on the side chain of a lysine.

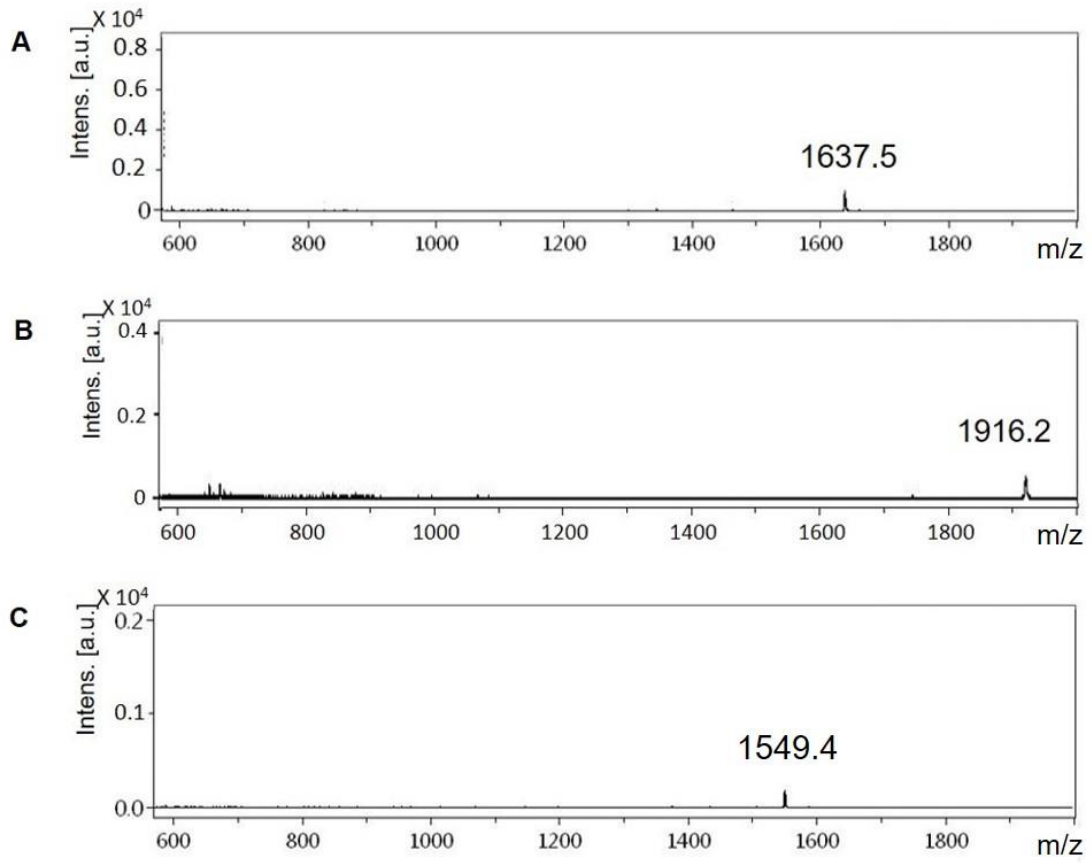

Figure 2.4. MALDI-TOF mass spectrum of the purified probes. (A) Probe **1** (B) Probe **2** (C) Probe **3**

2.2.2 Specific binding of the folate-NIR probe with confocal laser scanning microscopy

First *in vitro* experiments were performed to confirm the ability of the probe to specifically bind FR-expressing cells. FR (+) KB cells and FR (-) A549 cells were incubated with probe **1**. As shown in Figure 2.5, red fluorescence was only observed on the surface of FR (+) KB cells, A549 confirming the successful binding of the probe to FR. No fluorescence was observed on FR (-)cells, which confirms specific binding of the probe through the folate ligand to FR. These findings confirm that introduction of the fluorophore and palmitoyl groups did not hamper the recognition of the folate moiety against its receptor on the cell.

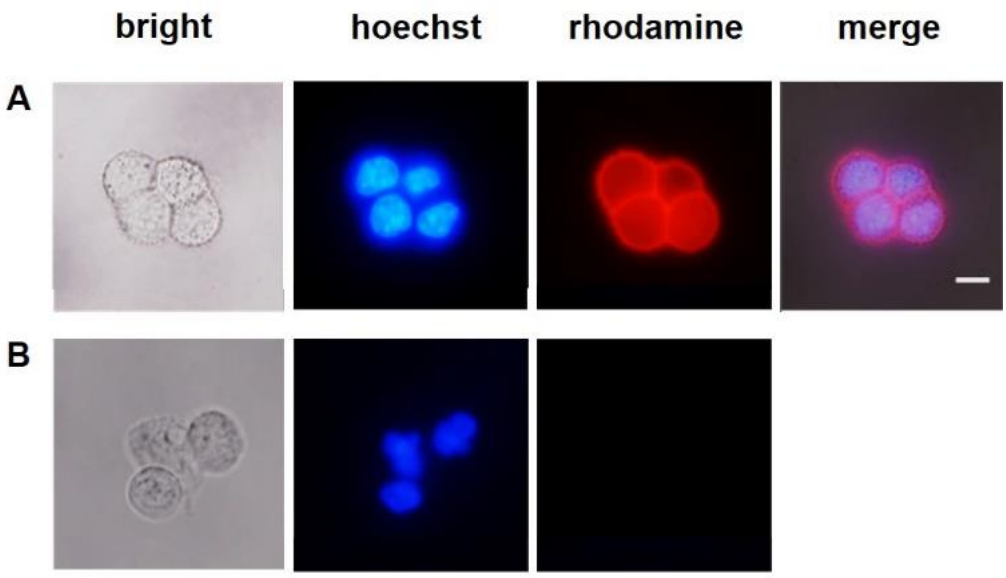

Figure 2.5. Specific binding of the folate-NIR probe to FR (+) KB cells. (A) Specific binding of the synthesized probe **1** to the folate receptor on FR (+) KB cells. (B) Absence of binding of probe **1** to FR (-) A549 cells. The scale bar represents 10 μm.

2.2.3 *In vivo* tumor-targeted imaging

Mice models bearing with FR (+) KB or FR (-) A549 tumors were intravenously injected with 1.5 nmol of probe **2** in the presence or absence of a 100-fold molar excess of free folate [29]. Images were acquired at various time points post-injection (p.i.) (Figure 2.6). The fluorescence intensity in the tumor as a function of time is plotted in Figure 2.6B and Figure 2.6D for KB and A549 tumor bearing mice, respectively. As shown in Figure 2.6A, FR (+) KB tumor-bearing mice that were injected only with probe **2** initially showed biodistribution of the probe in the whole body and then showed tumor accumulation at 1 h after the injection. After 6 h, probe **2** kept accumulating only in the tumor and liver, while it cleared from other parts of the body. After 12 h, accumulation of the probe with a high contrast was only observed in FR-expressing tumors, while the signal in liver disappeared. However, in FR (+) KB tumor-bearing mice in which the probe was co-injected with an excess amount of free folate, biodistribution and tumor accumulation of the probe was significantly suppressed. As shown in Figure 2.6A, co-presence of an excess amount of free folate largely inhibited specific binding of probe **2** to FR-expressing tumor cells. The probe also showed poor biodistribution in A549 tumor cells lacking FR (Figure 2.6C). Quantified data of the probe accumulation in tumor also established the probe specificity via the folate ligand-receptor interaction. As shown in Figure

2.6B, the tumor-to-normal tissue (T/N) ratio was reduced more than 75% by co-injection of excess folate.

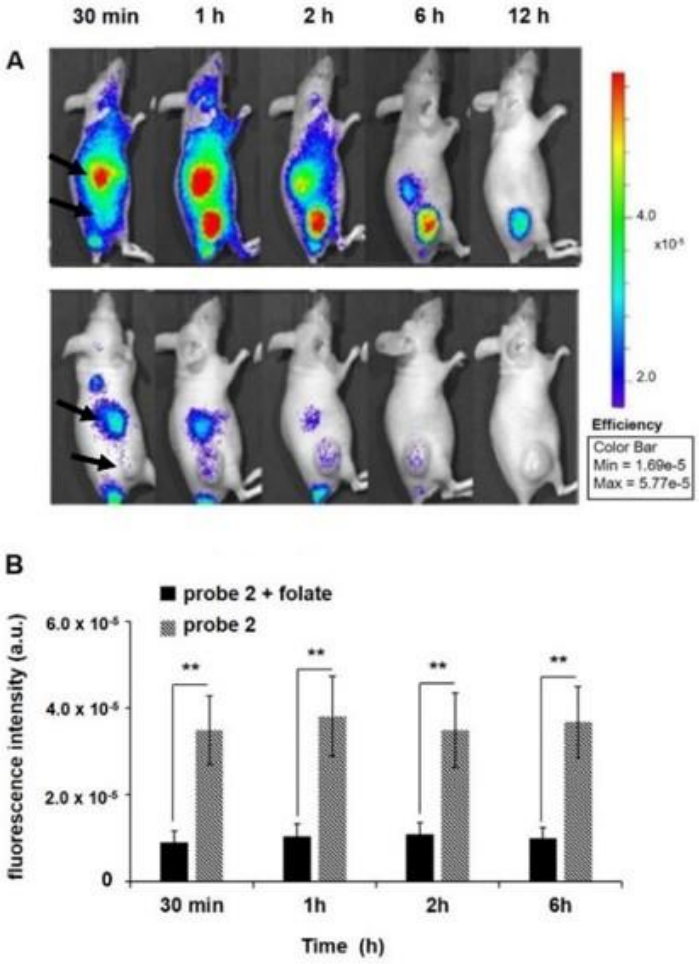

Figure 2.6. *In vivo* study of probe specificity. (A) Whole-body NIR fluorescence imaging of FR (+) KB tumor-bearing mice injected with 1.5 nmol of probe 2 in the absence (upper panel) or presence (lower panel) of 100-fold molar excess of free folate at 30 min, 1, 2, 6, and 12 h p.i. (B) ROI fluorescence intensity of the tumor as a function of time after injection of 1.5 nmol of probe 2 in the absence or presence of 100-fold of excess amount of free folate. Results are expressed as mean ± SD (n = 3). **P < 0.01, compared with no treatment. (C) Whole-body NIR fluorescence imaging of FR (-) A549 tumor-bearing mice injected with 1.5 nmol of probe 2 in the absence (upper panel) or presence (lower panel) of 100-fold molar excess of free folate at 30 min, 1, 2, 6, and 12 h p.i. (D) ROI fluorescence intensity of the tumor as a function of time after injection of 1.5 nmol of probe 2 in the absence or presence of 100-fold of excess amount of free folate. Results are expressed as mean ± SD (n = 3). Statistical results were in comparison with no treatment. N.S.: not significant. Arrows in each panel show liver and the tumor, respectively. (C) and (D) are continued on the following page.

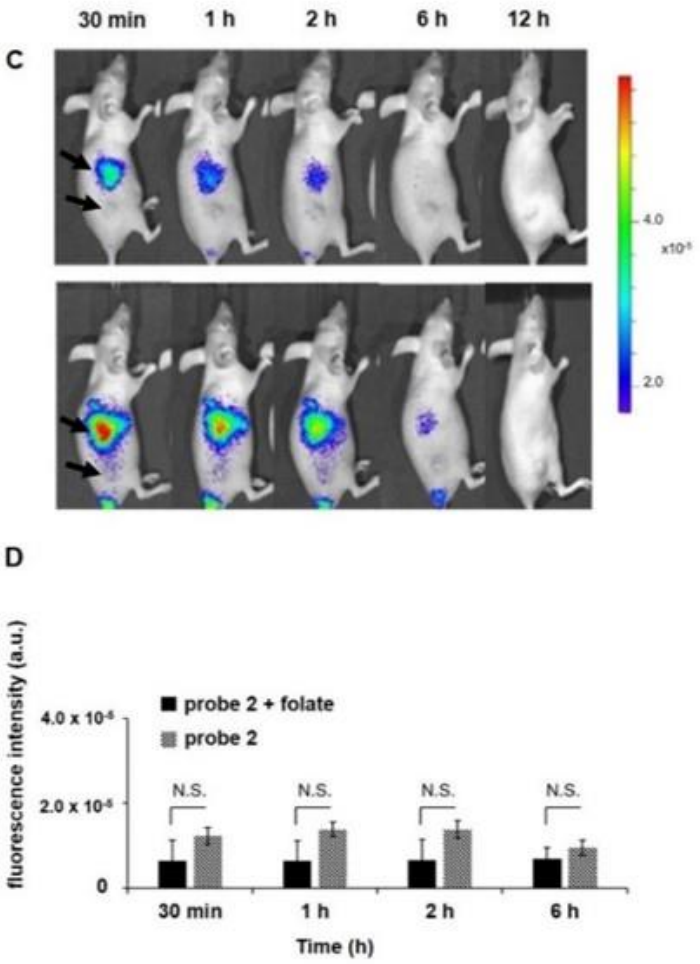

Figure 2.6. continued

Organ distribution of the probe also indicated the high specificity of the probe to the FR (+) KB tumor (Figure. 2.7). Three out of four mice in each group were sacrificed 6 h post injection (p.i). Only one mouse was kept until 12 h for imaging. Tumor, organs, and tissues including liver, lung, kidneys, spleen, heart, and blood were excised from mice. *Ex vivo* imaging and evaluation of dissected tissues from mice with probe **2** with or without co-injection of free folate revealed that the probe mainly distributed in tumor and kidney. A lesser extent of distribution was observed in liver, and the probe was detected at very low levels in other tissues. Quantification of fluorescence confirmed that in FR-expressing KB tumor-bearing mice, a high intensity of probe fluorescence could be detected in the tumor, while co-injection of free folate significantly attenuated probe accumulation in the same type of tumor (Figure. 2.7B).

The obtained results also showed that in addition to the accumulation of probe **2** in the tumor, probe **2** also distributed in kidney and liver. Accumulation of probe in the liver is possibly due to the large fenestrations of liver's capillary epithelium (size of 100 to 150 nm depending on the animal species), which allows almost unrestricted passage of plasma components to the perisinusoidal space of liver [13, 32]. Considerable high probe accumulation in kidneys also could have been caused by the presence of high-affinity folate receptors in proximal tube cells of kidneys [33-35].

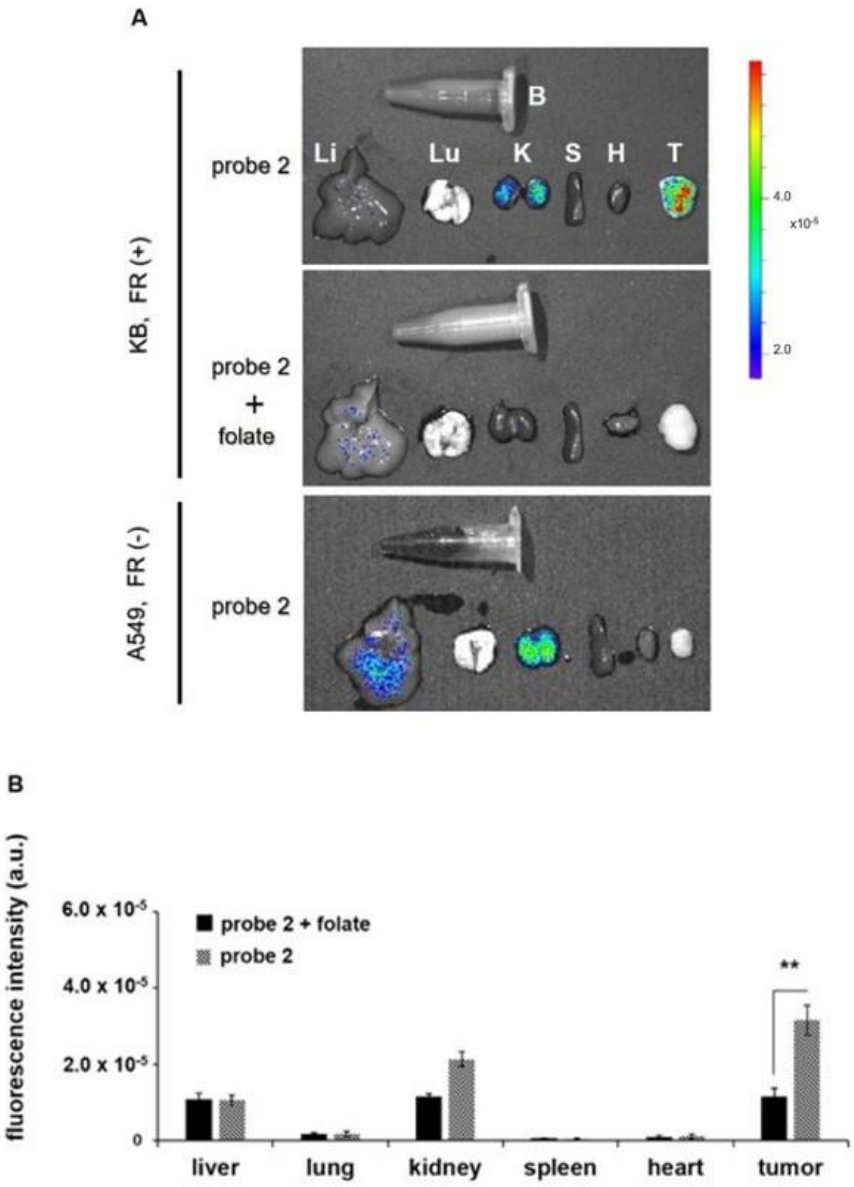

Figure 2.7. Representative fluorescence images of dissected KB and A549 tumors and major organs after noninvasive imaging at 6 h p.i. (A) Fluorescence image of dissected organs. B = blood, Li = liver, Lu = lungs, K = kidney, S = spleen, H = heart, T = tumor. KB tumor-bearing mice injected with 1.5 nmol of probe **2** in the absence (upper panel) or presence (middle) of 100-fold molar excess of free folate at 30 min, 1, 2, 6, and 12 h p.i. Lower panel indicates same image of organs from FR (-) A549 tumor-bearing mice. (B) ROI fluorescence analysis of dissected tumors and major organs after noninvasive imaging at 6 hours p.i. in FR (+) KB tumor-bearing mice in the absence or presence of excess folate. Results are expressed as mean ± SD (n = 3). **P < 0.01, compared with no treatment.

2.2.4 Effect of the alkyl chain moiety of the probe on blood circulation

In this study, I designed the probe based on the high binding affinity of the free fatty acid to the hydrophobic pockets of HSA. To examine whether the introduced palmitoyl in the probe molecule can serve as ligand against circulating HSA, 1.5 nmol of probe **2** or probe **3** (without palmitoyl) were injected in FR (+) KB-tumor bearing mice (Figure. 2.8). Fluorescence images were acquired at 30 min, 1, 2, 6, 18 and 24 h post-injection. Results indicated that probe **2** accumulated and had long retention in tumor likely through the ligand-receptor interaction. Probe **3** also accumulated in the tumor, but retention and accumulation in the tumor were shorter than that of probe **2** (Figure 2.8). Although the long retention of the probe in tumor may be caused by the effective binding of the folate ligand to its receptor on KB cells, obtained long circulation also contribute due to the efficient supply of the probe to the tumor with keeping high concentration of the probe in blood. In fact, the control probe without the palmitoyl group (probe **3**), showed poor circulation in mice, with a decreased retention of the fluorescent signal in the tumor compared with probe **2**. Together, the obtained results suggest that the design of the imaging probe with reversible binding to HSA that was introduced in this study may be an effective tool for cancer imaging.

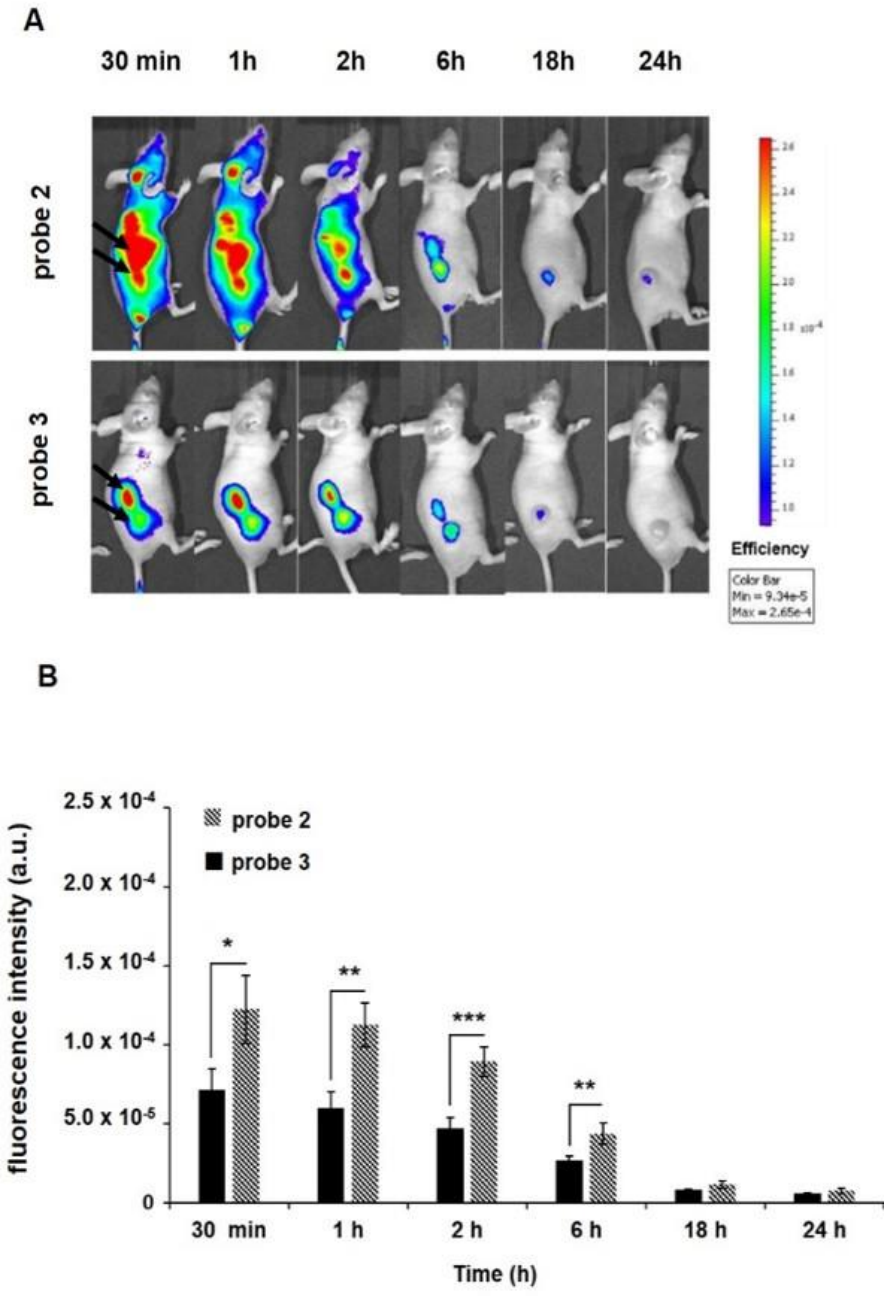

Figure 2.8. Biodistribution of probe **2** and probe **3** in time-course imaging. (A) Whole-body NIR fluorescence imaging of FR (+) KB tumor-bearing mice injected with 1.5 nmol of probe **2** (upper panel) or probe **3** (lower panel) 30 min, 1, 2, 6, 18, and 24 h p.i. (B) ROI fluorescence intensity analysis of the whole body of mouse as a function of time after injection of probe **2** or probe **3** into FR (+) KB tumor-bearing mice. Results are expressed as mean ± SD (n = 3). ***P < 0.001, **P < 0.01, *P < 0.05, compared to no treatment. Arrows in each panel show liver and the tumor, respectively.

2.3 Summary

Development of improved tumor imaging probes is clinically desirable with the purpose of detecting presence of tumor lesions, monitoring tumor response to treatment or tumor staging. Using these improved imaging agents to localize tumor cells is an advantageous technique for surgeons to achieve a more efficient intraoperative diagnosis and debulking operation. In line with this, targeting certain receptors which are overexpressed in cancer cells is a potential strategy. By now, some imaging agents had been introduced. However, mainly these imaging agents suffer from short circulation half-life because of their small size. In my research, I will address this problem and seek to enhance circulation time of the probe and reaching to more efficient tumor imaging. Thus, I synthesized the probe with a simple synthesis scheme, in which folic acid (folate) at the N terminus and alkyl chain (palmitoyl) at the C terminus are considered. Folate moiety of the probe is expected to selectively bind to overexpressed folate receptor in cancer cells. On the other hand, it is hypothesized that via palmitoyl moiety of this synthesized probe, it can reversibly interact with hydrophobic pocket of serum albumin. This probe, being carried by serum albumin in the blood circulation would result in escaping from an early renal clearance and having high circulation half-life. It is protected from elimination via recognition by the neonatal Fc receptors (FcRn), which prevent its catabolism in endothelial cells and ensures protein reabsorption in kidneys by proximal tubules after glomerular filtration.

The incorporation of a long fatty acid in the design of folate-targeted fluorescence imaging molecules showed longer blood circulation and bioavailability in mice bearing folate receptor-positive tumors. This result can be explained by the reversible binding of this probe (probe **2**) to hydrophobic pockets of endogenous serum albumin. This approach is attractive to generate small fluorescence imaging probes with a better bioavailability and longer blood circulation, that can result in an improved imaging or therapy.

2.4 Experimental section

Materials

NovaSyn TGR resin (amine density of 0.24 mmol/g) and all Fmoc-protected amino acids were obtained from Novabiochem, Merck (Tokyo, Japan). 1-hydroxy-1H-benzotriazole hydrate ($HOBt \cdot H_2O$), O-(benzotriazol-1-yl)-*N*,*N*,*N*′,*N*′-tetramethyluronium hexafluorophosphate (HBTU), diisopropylethylamine (DIPEA), dichloromethane (DCM), 1-methyl-2-pyrrolidone (NMP), *N*-α-(9-fluorenylmethoxycarbonyl)-L-glutamic acid α-t-butyl ester (Fmoc-Glu-OtBu), *N*-α-(9-fluorenylmethoxycarbonyl)-*N*-ε-palmitoyl-L-lysine (Fmoc-Lys(Pal)-OH), and piperidine were obtained from Watanabe Chemical (Hiroshima, Japan). *N*,*N*-Dimethylformamide (DMF) was purchased from Kanto Chemical (Tokyo, Japan). Dimethyl sulfoxide (DMSO), ethanol and E-MEM and D-MEM mediums were purchased from Wako Pure Chemicals (Osaka, Japan). RPMI 1640 (folate-free) medium was purchased from Life Technologies. 11-bromoundecanoic acid, 5-chloro-1-pentyne and 1, 8-diazabicyclo [5,4,0]-7-undecene (DBU) were obtained from Tokyo Kasei Industry (Tokyo, Japan), and 5-(and 6)-carboxytetramethylrhodamine succinimidyl ester (NHS-Rhodamine) from Thermo Scientific. Sulfo-Cyanine7 NHS ester was obtained from Lumiprobe and Fmoc-8-amino-3, 6 dioxaoctanoic acid (Fmoc-miniPEG) was obtained from Peptides International. N^{10}-(Trifluoroacetyl) pteroic acid, human serum albumin and folate (folic acid) were purchased from Sigma-Aldrich. All reagents were used without further purification.

Synthesis of the folate conjugates

Probes were synthesized by standard Fmoc-chemistry using the NovaSyn TGR resin (amine density of 0.24 mmol/g), DIPEA as a base, HOBt/HBTU as coupling reagents, and a 20% solution of piperidine in DMF for deprotection of the Fmoc group. First, Fmoc-Lys(Palmitoyl)-OH was coupled onto the resin. Next, two miniPEG and a Lys-(Boc) were modified as spacer and fluorophore modification sites, respectively. The folate moiety was modified with two-step introduction of glutamic acid and N10-(trifluoroacetyl) pteroic acid. Since trifluoroacetyl, the protecting group of pteroic acid, is resistant to general deprotection with trifluoroacetic acid (TFA), one additional deprotection step was conducted; resin was

washed with DMF five times and with DCM five times and then it was incubated with 1 mol/L ammonium hydroxide solution/DMF (1:1, vol/vol) for 30 min for four times to cleave the trifluoroacetyl protecting group. The resin was washed three times with DCM and three times with n-hexane, and then dried in vacuum. Afterward, the conventional deprotection and cleavage from resin solution were done by TFA. To introduce the fluorescent group residue onto the lysine of the folate conjugate, Cy7-NHS ester in anhydrous DMSO (10 mg/ml) was added to a peptide solution of 11.6 mg/ml in DMSO at a 1.2:1 dye to peptide molar ratio. Next, 1.2 molar ratio of DIEA was added and the solution was mildly shaken overnight.

For the in vitro study, carboxytetramethyl rhodamine-NHS ester was used instead of Cy-7-NHS. Purification of the solid-phase synthesized peptides was carried out on an analytical reversed-phase high performance liquid chromatography (HPLC) system using C18 RP (250 × 4.6 mm 5 μm) column using a linear A-B gradient at a flow rate of 1.16 mL/min, where eluent A was 0.1% TFA in water and eluent B was 0.1% TFA in acetonitrile. UV absorbance at 220 nm, 552 nm, and 740 nm was monitored. Purity analysis of the purified probes was carried out on an analytical reversed-phase high performance liquid chromatography (HPLC) system using C18 RP (100 × 4.6 mm 5 μm) column using a linear A-B gradient at a flow rate of 1 mL/min, where eluent A was 0.1% TFA in water and eluent B was 0.1% TFA in acetonitrile. B eluent with gradient of 25-70 in 45 minutes, 40-70% in 30 minutes and 20-50% in 30 minutes was run for the probe 1, 2 and 3, respectively. UV absorbance at 220, 552 nm and 740 nm was monitored. Calculated purity for the probes 1, 2 and 3 are 78%, 80% and 81%, respectively.

Cell lines and cell culture

The epidermal mouth carcinoma HeLa-contaminated KB cell line that overexpresses folate receptor (FR-α (+)) was cultured in E-MEM. The A549 cell line, which is negative for folate receptor (FR-α (-)) was cultured in D-MEM. Mediums contained 10% fetal bovine serum (FBS), 100 U/mL penicillin, 100 μg/mL streptomycin, and 0.25 g/mL amphotericin B (all from Gibco Invitrogen Co., Grand Island, NY, USA). Cells were cultured in a humidified atmosphere containing 5% CO_2 and 95% air at 37°C.

Probe binding assays

KB and A549 cells were seeded at a density of 5000 cells per well in a 96 well glass plate in 100 μl of RPMI 1640 (folate-free) medium. After 24 h, wells were washed twice with 100 μl DPBS. Next, 100 nM of probe 1 in 100 μl medium was added to wells. The plate was incubated on ice for 30 min. The solution was removed and cells were washed twice with 100 μl DPBS. Next, 100 μl of medium was added and the nuclei were stained with Hoechst 33342. After washing, cells were observed by fluorescence microscopy. Images were obtained by using manufacturer-specified laser excitation wavelengths and emission filter sets.

In vivo mouse model

Animal studies were performed in accordance with the Guidelines for Animal Care and Use Committee at Kyushu University (Fukuoka, Japan). Female 5-week-old BALB/c nude mice were inoculated with a dorsal, subcutaneous injection of 1.6×10^7 KB cells and 6.5×10^7 A549 cells in 50 μL of Matrigel (BD Biosciences, Bedford, MA, USA) and 50 μL of PBS per animal. Tumors were allowed to grow for about two weeks to a mean diameter of approximately 10 mm.

Fluorescent imaging of tumor inoculated mice

Fluorescence imaging was performed using a cooled IVIS® CCD camera (Xenogen, Alameda, CA, USA) and analyzed with Living Image software. All fluorescence images were acquired with a 2 sec exposure. For quantitative comparison, regions of interests (ROIs) were drawn over the tumor or whole body and the results are presented as the mean ± standard deviation (SD) for a group of three animals. Excitation and emission maximum wavelengths of Cy7 are 740 nm and 773 nm, respectively. The most suitable filter in the IVIS® Imaging System covered the excitation passband of 710–760 nm and emission passband of 810–875 nm.

2.5 References

[1] A. B. Chinen, C. M. Guan, J. R. Ferrer, S. N. Barnaby, T. J. Merkel and C. A. Mirkin, *Chem. Rev.*, 2015, **115**, 10530−10574

[2] J. Condeelis and R. Weissleder, *Cold Spring Harb. Perspect. Biol.*, 2010, **2**, 1-22.

[3] G. M. van Dam, G. Themelis, L. M. a Crane, N. J. Harlaar, R. G. Pleijhuis, W. Kelder, A. Sarantopoulos, J. S. de Jong, H. J. G. Arts, A. G. J. van der Zee, J. Bart, P. S. Low and V. Ntziachristos, *Nat. Med.*, 2011, **17**, 1315–9.

[4] M. E. L. van der Burg, M. van Lent, M. Buyse, A. Kobierska, N. Colombo, G. Favalli, A. J. Lacave, M. Nardi, J. Renard and S. Pecorelli, *Obstet. Gynecol. Surv.*, 1995, **50**, 516–518.

[5] N. J. Harlaar, W. Kelder, A. Sarantopoulos, J. Bart, G. Themelis, G. M. Van Dam and V. Ntziachristos, *Gynecol. Oncol.*, 2013, **128**, 590–595.

[6] L. E. Kelderhouse, V. Chelvam, C. Wayua, S. Mahalingam, S. Poh, S. A. Kularatne and P. S. Low, *Bioconjug. Chem.*, 2013, **24**, 1075–1080.

[7] A. Becker, C. Hessenius, K. Licha, B. Ebert, U. Sukowski, W. Semmler, B. Wiedenmann and C. Grötzinger, *Nat. Biotechnol.*, 2001, **19**, 327–331.

[8] P. S. Low, W. A. Henne and D. D. Doorneweerd, *Acc. Chem. Res*, 2008, **41**, 120-129.

[9] P. S. Low and S. A. Kularatne, *Curr Opin Chem Biol*, 2009, **13**, 256–262.

[10] P. S. Low and A. C. Antony, *Adv. Drug Deliv. Rev.*, 2004, **56**, 1055–1058.

[11] J. Sudimack, R. J. Lee, *Adv. Drug Deliv. Rev.*, 2000, **41**, 147–162.

[12] F. Alexis, E. Pridgen, L. K. Molnar and O. C. Farokhzad, *Mol. Pharm.*, 2008, **5**, 505–515.

[13] N. Bertrand and J. C. Leroux, *J. Control. Release*, 2012, **161**, 152–163.

[14] H. Kobayashi, R. Watanabe and P. L. Choyke, *Theranostics*, 2014, **4**, 81–89.

[15] V. Torchilin, *Adv. Drug Deliv. Rev.*, 2011, **63**, 131–135.

[16] H. Maeda, H. Nakamura and J. Fang, *Adv. Drug Deliv. Rev.*, 2013, **65**, 71–79.

[17] D. Sleep, J. Cameron and L. R. Evans, *Biochim. Biophys. Acta*, 2013, **1830**, 5526–5534.

[18] G. J. Quinlan, G. S. Martin and T. W. Evans, *Hepatology*, 2005, **41**, 1211–1219.

[19] B. Elsadek and F. Kratz, *J. Control. Release*, 2012, **157**, 4–28.

[20] Y. R. Zheng, K. Suntharalingam, T. C. Johnstone, H. Yoo, W. Lin, J. G. Brooks and S. J. Lippard, *J. Am. Chem. Soc.*, 2014, **136**, 8790–8798.

[21] F. Kratz, *J. Control. Release*, 2008, **132**, 171–183.

[22] J. R. Levick, *Arthritis Rheum.*, 1981, **24**, 1550–1560.

[23] A. Wunder, U. Muller-Ladner, E. H. Stelzer, J. Funk, E. Neumann, G. Stehle, T. Pap, H. Sinn, S. Gay and C. Fiehn, *J Immunol*, 2003, **170**, 4793–4801.

[24] G. Stehle, H. Sinn, A. Wunder, H. H. Schrenk, J. C. M. Stewart, G. Hartung, W. Maier-Borst and D. L. Heene, *Crit. Rev. Oncol. Hematol.*, 1997, **26**, 77–100.

[25] A. A. Spector, *J. Lipid Res.*, 1975, **16**, 165–179.

[26] N. Parker, M. J. Turk, E. Westrick, J. D. Lewis, P. S. Low and C. P. Leamon, *Anal. Biochem.*, 2005, **338**, 284–293.

[27] M. S. Dennis, H. Jin, D. Dugger, R. Yang, L. McFarland, A. Ogasawara, S. Williams, M. J. Cole, S. Ross and R. Schwall, *Cancer Res.*, 2007, **67**, 254–261.

[28] M. Fasano, S. Curry, E. Terreno, M. Galliano, G. Fanali, P. Narciso, S. Notari and P. Ascenzi, *IUBMB Life*, 2005, **57**, 787–96.

[29] B. Vaitilingam, V. Chelvam, S. A. Kularatne, S. Poh, W. Ayala-Lopez and P. S. Low, *J. Nucl. Med.*, 2012, **53**, 1127–34.

[30] C. Chen, J. Ke, X. Edward Zhou, W. Yi, J. S. Brunzelle, J. Li, E. L. Yong, H. E. Xu and K. Melcher, *Nature*, 2013, **500**, 486–489.

[31] G. V. Richieri, A. Anel and A. M. Kleinfeld, *Biochemistry*, 1993, **32**, 7574–7580. OK

[32] E. Wisse, F. Jacobs, B. Topal, P. Frederik and B. De Geest, *Gene Ther.*, 2008, **15**, 1193–1199.

[33] J. A. N. Holm, S. I. Hansen, M. Høier-madsen and L. Bostad, *Kidney Int.*, 1992, **41**, 50–55.

[34] H. Birn, O. Spiegelstein, E. I. Christensen and R. H. Finnell, *J. Am. Soc. Nephrol.*, 2005, **16**, 608–615.

[35] S. F. Knight, K. Kundu, G. Joseph, S. Dikalov, D. Weiss, N. Murthy and W. R. Taylor, *J. Am. Soc. Nephrol.*, 2012, **23**, 793–800.

CHAPTER 3

Enhancement of peptide-based ligands affinity to human serum albumin

3.1 Introduction

Strategies to improve the blood half-life of peptide or protein drugs are highly demanded because they often display a half-life of a few minutes, mainly due to their low molecular mass or enzymatic degradation which results in a rapid clearance by renal filtration. Such strategies can minimize the dosage frequency of the peptide drugs. Conjugation of peptides to polyethylene glycol (PEG) has been used conventionally for this purpose [1-3]. However, repeated administration of PEGylated peptides is known to be associated with immunogenicity against PEG [4]. Newer strategies include genetically fusion of peptides and proteins to Fc-domain of immunoglobulin G (IgG), as this domain mediates the recycling through FcRn. As a result, it exhibits longer long half-lives close to the original IgG, which is about 3-4 weeks [5, 6]. Nonetheless, the analyzed Fc-fusion proteins (abatacept, alefacept, and etanercept) exhibited a 2–3-fold lower affinity for FcRn than various humanized antibodies, which was also reflected by a shorter half-life. It is speculated that the fused receptor domains interfere with the FcRn-binding site [7].

Human serum albumin (HSA), the most abundant protein in the blood (0.6 mM), has a long serum half-life of 19 days. This long half-life is due to the avoidance of lysosomal degradation via the endocytic salvage pathway [8, 9]. HSA is the natural carrier for many exogenous and endogenous substances [10]. Owing to these unique features, HSA has recently been utilized to improve the blood half-life of peptide drugs [11, 12]. As shown in Figure 3.1A, HSA is composed of three homologous domains I-III and each one divided into subdomains A and B. As HSA possesses seven hydrophobic pockets against relatively long fatty acids [13-15], alkyl modification of peptide drugs enables reversible binding with HSA to enhance the blood half-life. Clinically used insuline detemir (Levemir®), insulin (Degludec), and Liraglutide (Victoza®) are based on a single alkylation on the peptide sequence of human insulin or glucagon-like-1 peptide (Figure 3.2A and 3.2B) [16, 17]. This modification has extended these therapeutic peptides half-life from few minutes to hours and consequently reduced the dosage frequency [11, 17, 18]. However, generally, the binding affinity of alkylated peptides to HSA is attenuated by at least one order of magnitude comparing with the

original free fatty acid, probably due to the increase in overall hydrophilicity of the fatty acid and/or steric repulsion associated with the rest of peptides [16].

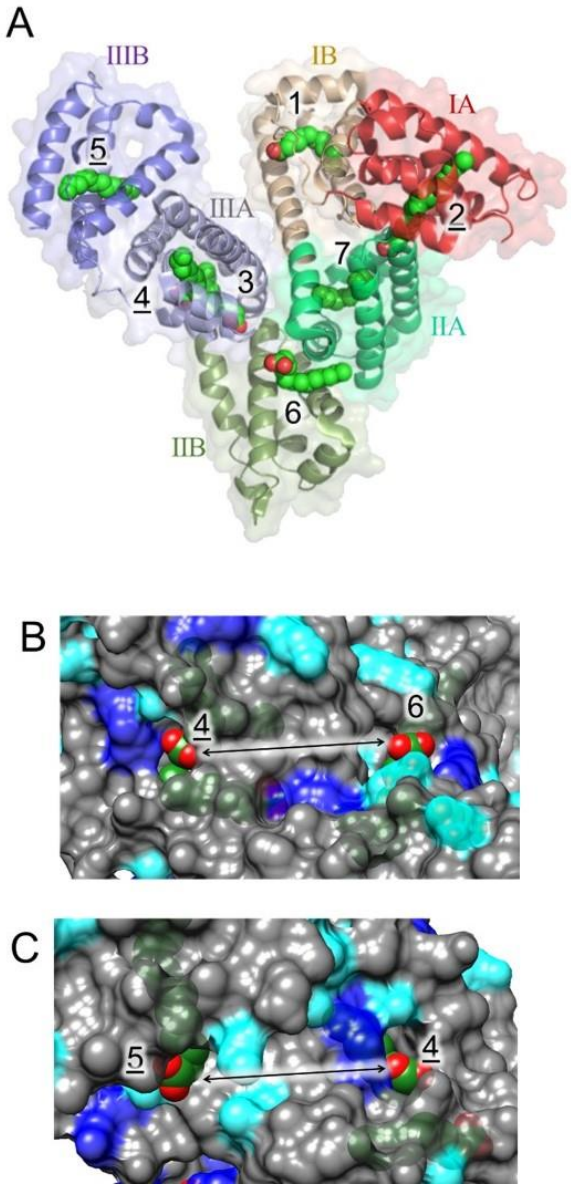

Figure 3.1. (A) Crystal structure of myristate bound HSA (PDB: 1eg7). Pocket number with underbar are strong binding pockets for hydrophobic compounds. (B) and (C) show cross-linkable pockets. Residues shown in blue and cyan indicate arginine and lysine residues, respectively. The distance between two pockets is almost equal and is about 2.2 nm.

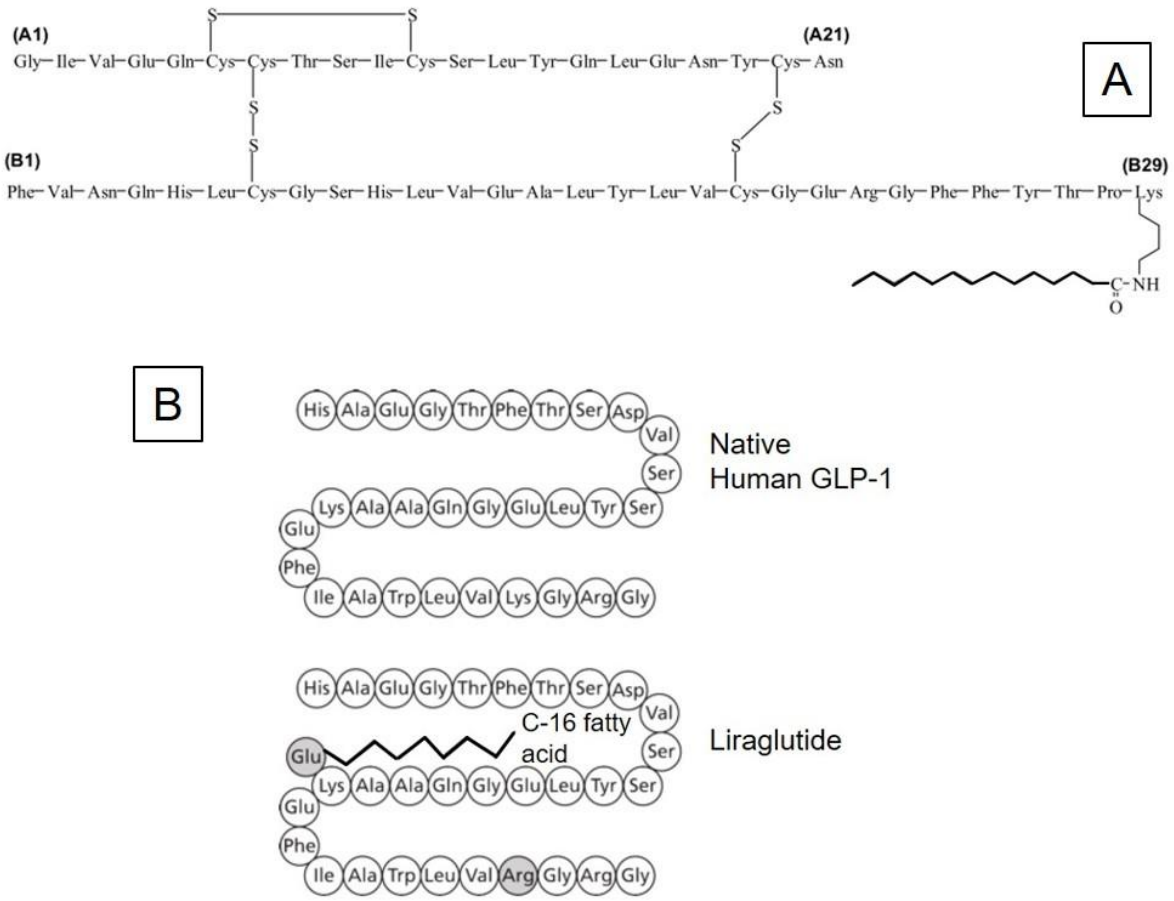

Figure 3.2. (A) Single alkylated insulin degludec (B) Single alkylated liraglutide.

In this chapter, I proposed a design of peptide-based ligands to HSA, in which two alkyl chains are introduced on to an appropriate spacer, expecting to enhance the binding affinity to HSA. Among the seven pockets of HSA against fatty acids, pockets 2, 4, and 5 are reported to be relatively strong [14]. As shown in Figure 3.1B and C, combinations of pockets 4 and 6 or 4 and 5 are expected to be cross-linkable by two alkyl groups because their entrance confronts a same face of HSA with similar close proximity (~2 nm). There is a cleft connecting two pockets in both combinations, which seems to be preferable to crosslink the pockets. Based on these structural features of HSA, I designed four kinds of peptide-based ligands shown in Figure 3.3. Here, binding affinity and blood circulation property of the peptides were examined to show the validity of the dual alkylation design for the stronger binding to HSA.

3.2 Results and discussion

3.2.1 Design and synthesis of the albumin-binding peptide

Four kinds of peptides were designed as shown in Figure 3.3. Peptide **1** and **3** have two alkyl groups (C14 or C16) which are connected with a linker possessing four ionizable carboxyl groups. These four carboxyl groups are expected to interact with cationic residues (Lys and Arg) existing in the connecting cleft of the binding pockets (Figure 3.1B and C), which are known to enhance the binding affinity against fatty acids [19]. The length of the peptide linker with extended conformation is 2.4 nm, which will be enough to crosslink the hydrophobic pockets. Peptide **2** is a control peptide possessing one alkyl group. Peptide **2** is a control peptide possessing one alkyl group. Peptide **4** is another control peptide whose linker includes flexible oligoethyelene glycol units with two-times longer length than that of all other peptides. For *in vivo* evaluation, Cyanine7 modified peptide **1** and **2** were also synthesized. All peptides were synthesized by solid-phase peptide synthesis with Fmoc chemistry. Chemical structures of peptide **1**, **2**, **3**, **4**, **1**-Cy7 and **2**-Cy7 are (11-amino-3,6,9-trioxyundecanyl)-E(myristoyl)DγEβADE(myristoyl)-OH and (11-amino-3,6,9-trioxyundecanyl)-GDγEβADE(myristoyl)-OH, (11-amino-3,6,9-trioxyundecanyl)-E(palmitoyl)DγEβADE(palmitoyl)-OH, (11-amino-3,6,9-trioxyundecanyl)-E(palmitoyl)DγE(miniPEG3)$_2$DE(palmitoyl)-OH, Cy7-(11-amino-3,6,9-trioxyundecanyl)-E(myristoyl)DγEβADE(myristoyl)-OH, Cy7-(11-amino-3,6,9-trioxyundecanyl)-E(palmitoyl)DγEβADE(palmitoyl)-OH, respectively.

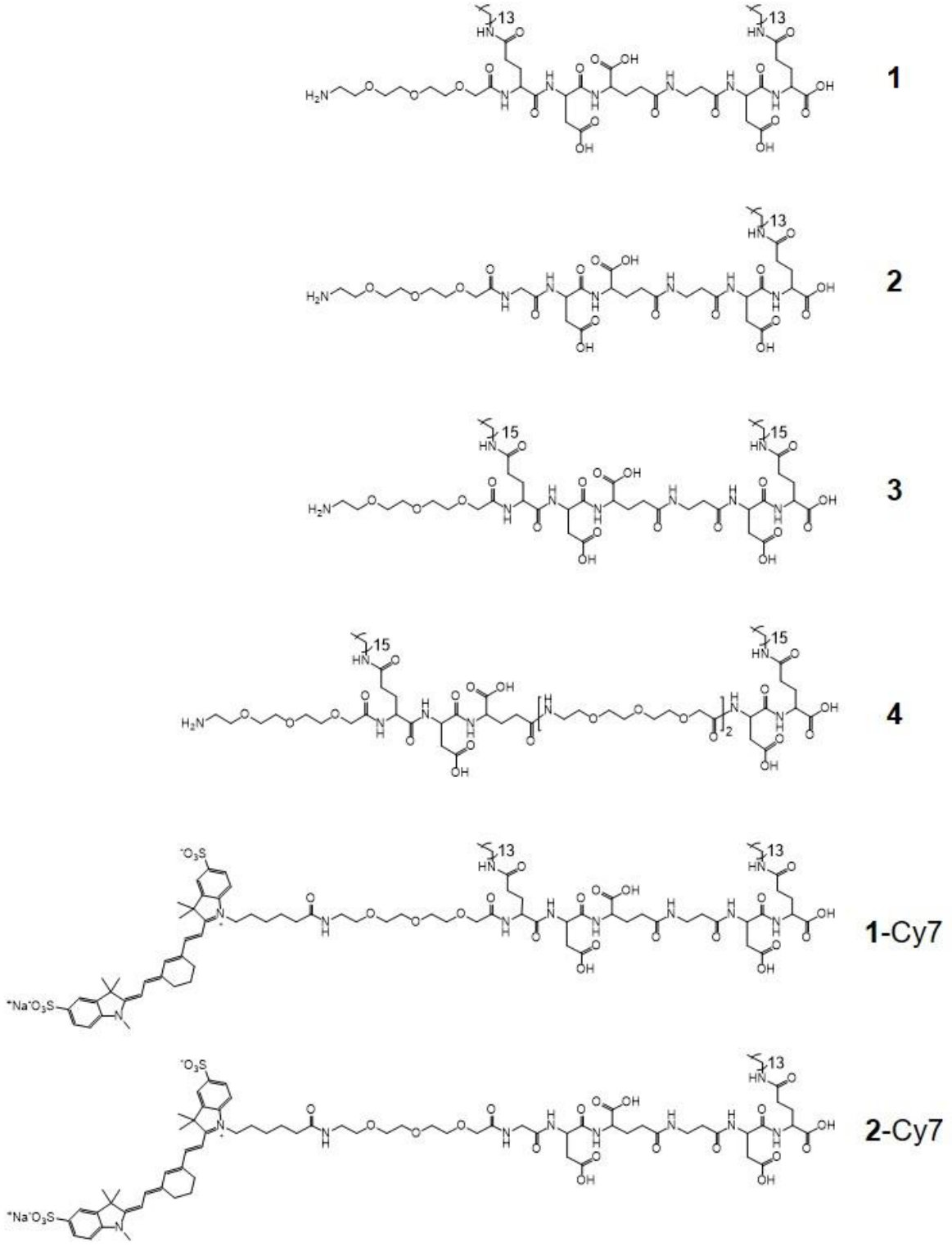

Figure 3.3. Chemical structure of the synthesized peptides.

3.2.2 Binding affinity determination by using fluorescence titration

To evaluate binding affinity of the synthesized peptides to HSA, I utilized a competitive replacement, using 8-Anilino-1-nephthalenesulfonic (ANS) fluorescence probe. As it can be seen in the Figure 3.4, ANS is basically non-fluorescent in aqueous media but shows strong fluorescence upon binding to the hydrophobic pocket of HSA or nonpolar solvents [20-22]. Thus, the replacement of ANS bound to HSA with ligands causes quenching of the ANS fluorescence. It has been reported that subdomain IIIA and IIA of HSA have the binding pockets of ANS to provide fluorescent property to ANS [23, 24]. Therefore, the fluorescence quenching is caused mainly by the competition between binding of the ligands with the ANS bound to the IIIA/IIA subdomain. Figure 3.5A shows results of competitive titration of HSA/ANS complex with the peptides or myristic acid. Figure 3.5A was converted to Figure. 3.5B, in which the replaced fraction of ANS (θ) was plotted as a function of the free ligand concentration. It is assumed that the decrease in the fluorescence intensity is a direct consequence of the release of ANS from its fluorescence-sensitive binding sites in HSA. The results on Figure 3.5B were fitted based on the Langmuir binding isotherm [25],

$$\theta = \frac{\eta K_d(\text{rel})[\text{Ligand}_{free}]}{1+K_d(\text{rel})[\text{Ligand}_{free}]} \qquad (1)$$

$$K_d = \frac{K_d(\text{rel}) \times K_d(\text{ANS})}{[\text{ANS}]} \qquad (2)$$

in which η and $K_{d(rel)}$ are the replaced fraction of ANS and the relative dissociation constant of each ligand against ANS, respectively. Binding parameters of ligands are summarized in the Table 3.1. Absolute K_d value of each ligand is calculated from the Eq. (2), in which $K_{d(ANS)}$ was determined experimentally by titration of HSA solution with ANS to be 2.7×10^{-7} M. As shown in Figure. 3.5A and 3.5B, myristic acid almost completely replaced to ANS bound to HSA and its K_d is calculated to be 1.7×10^{-7} M, which these calculated K_d values are in agreement with reported values [21, 26, 27]. Peptide **2** which has a single alkyl group was found to have K_d of 8.9×10^{-6} and induced only ca. 30% quenching of ANS even at its

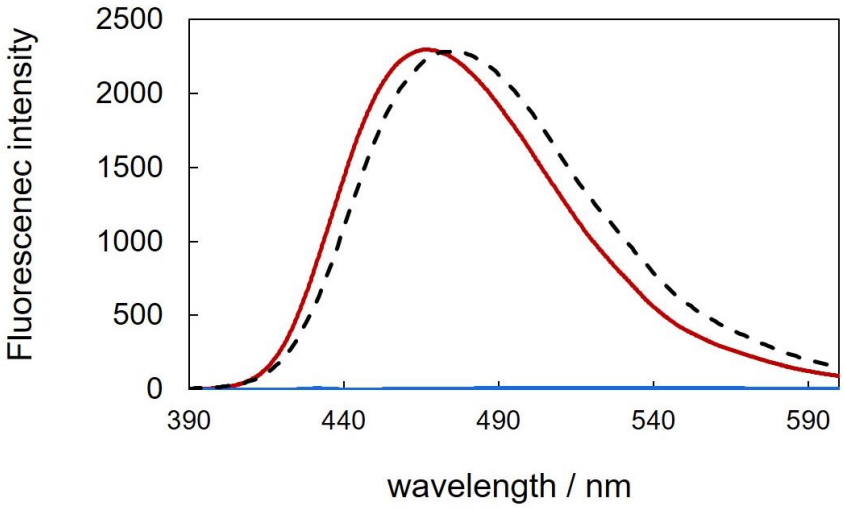

Figure 3.4. Fluorescence spectra of ANS in different conditions: red solid-curve; ANS bound to HSA in phosphate buffer, blue solid-curve; ANS in HSA-free phosphate buffer, black dot-line; ANS in HSA-free methanol.

maximum concentration (200 μM). The weak binding affinity of peptide **2** is probably due to the solubility increase of the alkyl group resulted from the modification of hydrophilic linker or the steric hindrance caused by the linker. K_d value of dual alkylated peptide **1** and **3** greatly improved the binding affinity to HSA which are calculated to be 4.0×10^{-8} M and 1.4×10^{-7} M, respectively. The improved binding affinity of peptide **1** and **3** will be explained by their simultaneous binding to two pockets of HSA. It is interesting to note that the quenching of ANS by **1** and **3** was saturated around 60%. Reported numbers of bound ANS to the HSA subdomain IIIA and IIA are one and two, respectively [23, 28]. Assuming that the quantum yields of these three ANSs are equivalent, 60% quenching shows dissociation of two out of the three bound ANSs from HSA. The binding of peptide **1** and **3** to the pockets of 4 and 5 results in dissociation of only one ANS at IIIA, which cannot explain 60% quenching. While the binding of the peptides to the pockets 4 and 6 results in dissociation of one ANS in IIIA and one of two ANSs in IIA, which is matched with 60% quenching. Thus, peptide **1** and **3** will specifically bind to pocket 4 and 6. Incomplete quenching by peptide **1** and **3** shows that their binding affinity to the other pocket in IIA domain is not enough to replace the remaining ANS. It is a sharp contrast with the simple fatty acids like myristic acid, which can replace all the three fluorescent ANSs. I concluded that peptide **1** and **3** gained specificity in the binding pockets.

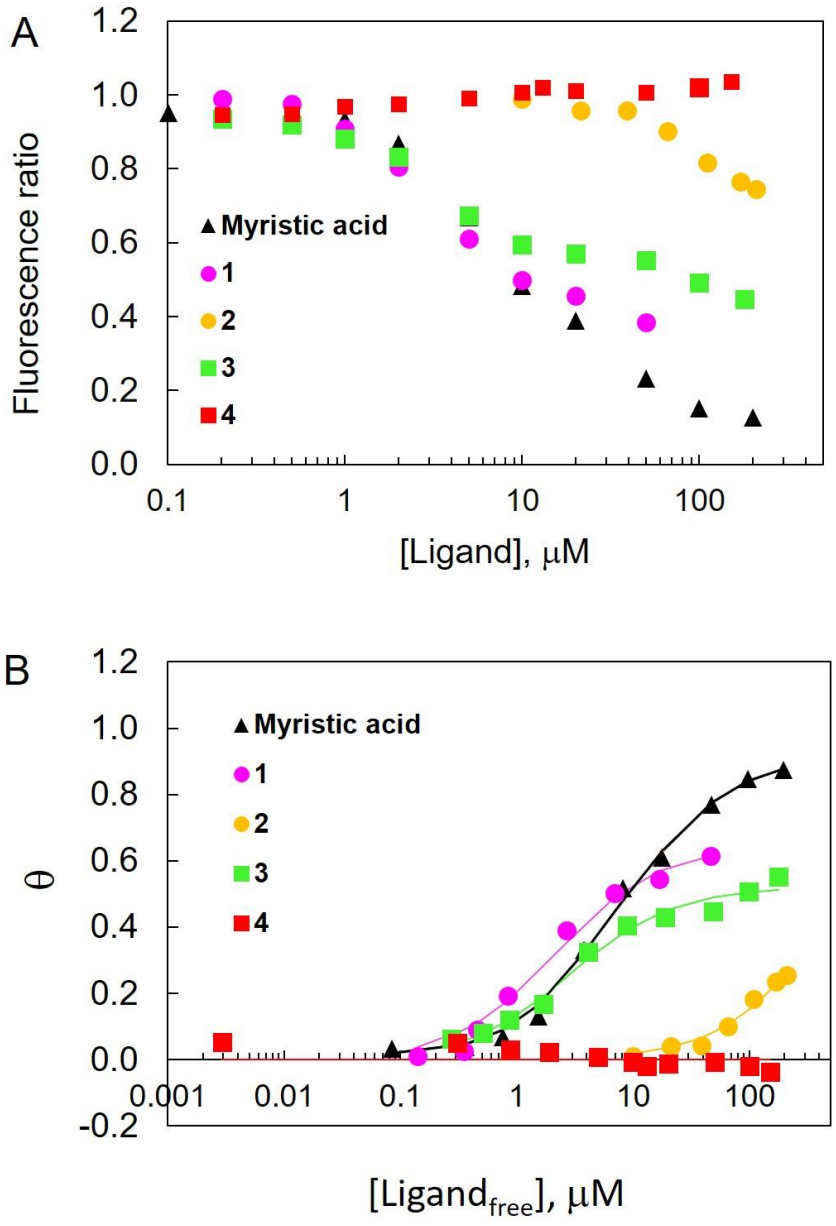

Figure 3.5. Competitive binding assay. (A) Inhibition of the ANS fluorescence intensity by each ligand. (B) Fraction of released ANS (θ) was plotted against the concentration of free ligand. The solid lines are the nonlinear least-squares fitted curve based on Langmuir binding isotherm. Concentrations of ANS and HSA were 15 and 2 μM, respectively.

Table 3.1. Binding parameters of myristic acid and synthesized peptides to HSA

	$K_{b(rel)}$	$K_{d(rel)}$	K_d	K_b
Myristic acid	1.0×10^{5}	9.1×10^{-6}	1.7×10^{-7}	5.9×10^{6}
1	4.5×10^{5}	2.1×10^{-6}	4.0×10^{-8}	2.4×10^{7}
2	2.0×10^{3}	4.8×10^{-4}	8.9×10^{-6}	1.1×10^{5}
3	1.2×10^{5}	8.0×10^{-6}	1.4×10^{-7}	6.7×10^{6}

Despite having a longer alkyl chain (C16), peptide **3** showed a similar binding affinity towards HSA with that of the peptide **1** (C14). This result is in agreement with previous results that the binding affinity of alkyl group to HSA does not increase when its length is more than 14 carbon atoms [16]. As in the case of peptide **4**, its flexible and two-times longer spacer completely spoiled its binding affinity towards HSA, indicating that designing the linker being complementary to the cleft connecting the pockets is crucial for the high binding affinity of the peptides to HSA.

3.2.3 Effect of peptide ligand on the fluorescence of ANS

In order to study the effect of peptide ligands on the fluorescence of ANS, I performed a titration of 15 μM free ANS solution (in the absence of HSA) with different concentrations of peptide 2. As it can be seen in the Figure 3.6, interaction of the peptide with ANS and the following enhancement of fluorescence intensity is negligible even at the highest concentration of peptide (210 mM) (2% of total fluorescence intensity). Thus, the effect of peptide **2** on the fluorescence of ANS is negligible.

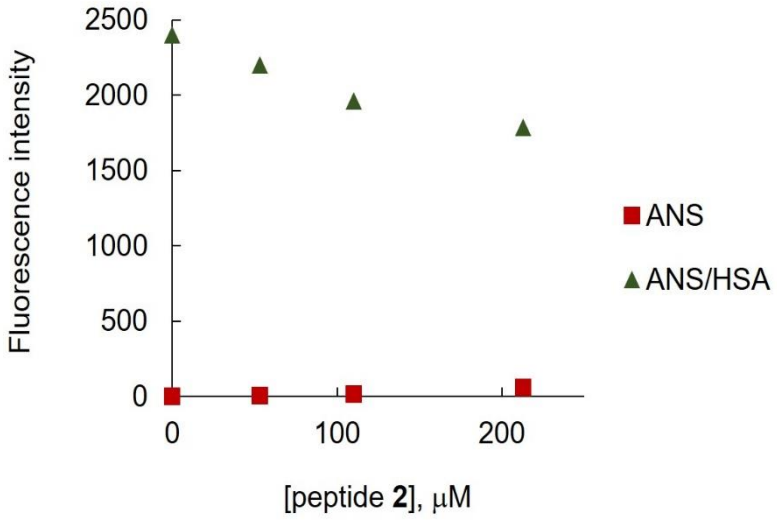

Figure 3.6. Change of ANS fluorescence intensity by addition of different concentration of peptide **2**, in the presence or absence of HSA. Concentrations of ANS and HSA were 15 and 2 μM, respectively.

3.2.4 Retention ability of dual alkylated peptide in the mice blood circulation

Retention ability of peptides **1** and **2** in the blood circulation of mice was examined by using the Cy7 modified peptides **1**-Cy7 and **2**-Cy7. Each peptide (2.1 nmol) dissolved in PBS was intravenously injected through the tail vein (4 mice per group). Blood samples were collected at 6 h post-injection. Protein fractions of the plasma were precipitated with acetonitrile to extract the peptides. Extracted peptides were redissolved in methanol. As shown in Figure 3.7, measured fluorescence intensity from extracted plasma samples showed a 3-fold higher fluorescence intensity of dual alkylated **1**-Cy7 compared to the single alkylated **2**-Cy7. This difference can be explained by a stronger binding ability of **1**-Cy7 to the serum albumin. No crystal structure of mouse serum albumin has so far been reported. But based on amino acid sequential studies, important residues for the binding of fatty acids are nearly completely conserved among all species, a similar binding behavior from human serum albumin and mouse serum albumin can be expected [29].

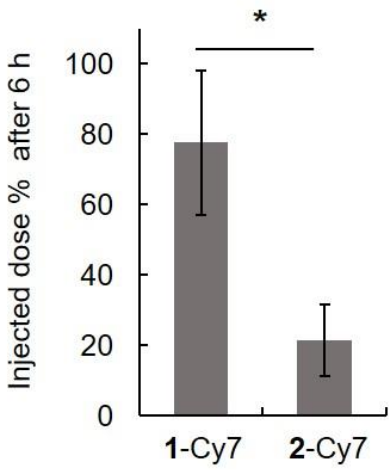

Figure 3.7. Retention of single and dual alkylated albumin binding peptides. Six hours after i.v. injection, fluorescence of the remaining peptide was measured. n = 4 for each group. *: $p < 0.05$

3.3 Summary

Therapeutic peptides and diagnostic agents with their molecular size below the renal clearance threshold suffer from a poor bioavailability and short blood circulation time. This results in an insufficient accumulation in the target site and a demand for higher dosage frequency. In this chapter, I reported a novel design of peptide-based ligand with a strong binding affinity to human serum albumin (HSA), which can be used as a tag to extend the blood circulation of the small size molecules. I designed these ligands with dual alkyl groups connected with a negatively charged spacer. By a competitive binding technique, it was found out that the designed dual alkylated peptides with the tuned and shorter spacer were able to specifically share the HSA's binding pockets 4 and 6 for fatty acids, with a significantly higher binding affinity than that of the single alkylated peptide. Additionally, Cy7 modified dual alkylated peptide showed higher retention in the mice blood circulation than that of a single alkylated peptide, suggesting higher binding affinity of the former type of peptide to mouse serum albumin. No crystal structure of mouse serum albumin has so far been reported. But based on amino acid sequential studies, important residues for the binding of fatty acids are nearly completely conserved among all species. Thus, a similar binding behavior from human serum albumin and mouse serum albumin is expected.

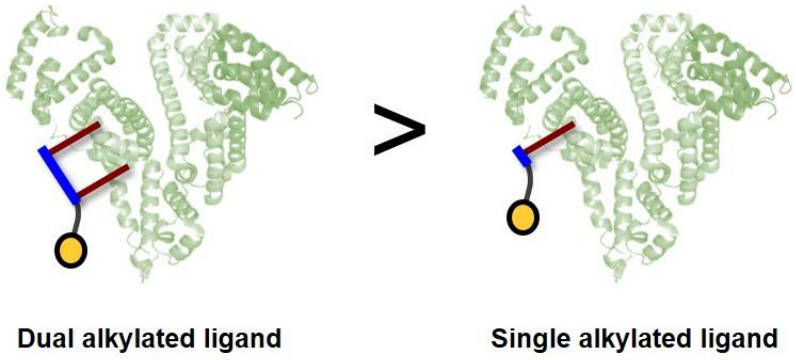

Figure 3.8. A new peptide-based ligand with two alkyl groups and appropriate peptide backbone showed much higher affinity than a ligand with a single alkyl group to human serum albumin.

3.4 Experimental section

Materials

NovaSyn TGA resin (amine density of 0.2 mmol/g), Fmoc-Glu(Odmab)-OH, Fmoc-Asp(OtBu)-OH and Fmoc-Gly-OH were obtained from Novabiochem, Merck (Tokyo, Japan). N-[1-(Cyano-2-ethoxy-2-oxoethylideneaminooxy) dimethylamino (morpholino)] uronium hexafluorophosphate (COMU), Fmoc-β-Ala-OH, Fmoc-Glu-OtBu, diisopropylethylamine (DIPEA), dichloromethane (DCM), 1-methyl-2-pyrrolidone (NMP), and piperidine were purchased from Watanabe Chemical (Tokyo, Japan). Pyridine, N,N-dimethyl-4-aminopyridine benzoic anhydride (DMAP) and N,N-diisopropylcarbodiimide (DIC) were obtained from Wako Pure Chemicals (Osaka, Japan). *Boc-11-amino-3,6,9-trioxaundecanoic acid•DCHA (Boc-mini-PEG3) and Fmoc-11-3,6,9-trioxaundecanoic acid (Fmoc-mini-PEG3) were purchased from Peptides International (Kentucky, USA). N,N-dimethylformamide (DMF) was purchased from Kanto Chemical (Tokyo, Japan).* All reagents were used without further purification. Fatty acid free human serum albumin and *myristic acid* were purchased from Sigma-Aldrich. Tetradecylamine, triisopropylsilane (TIS), hexadecylamine and sodium salt of 8-Anilino-1-naphthalenesulfonate (ANS•Na) were purchased from Tokyo Chemical Industry (Tokyo, Japan). Sample solutions were prepared using the water purified by Direct-Q® Water Purification System.

Synthesis of peptides 1-4, 1-Cy7, 2-Cy7

The peptides were synthesized manually by standard Fmoc chemistry using NovaSyn TGA resin (density of 0.2 mmol/g), DIEA as a base and COMU as coupling reagents. Deprotection of the N^{α}-Fmoc was carried out in 20% piperidine/DMF, followed by washings with dichloromethane (DCM) and dimethylformamide (DMF). Modification of peptides with tetradecylamine or hexadecylamine were conducted after deprotection of Dmab group of Glu in two steps; treatment of the resin bound peptide with 2% hydrazine monohydrate in DMF for 30 min followed by treatment of the resin with 5 mM sodium hydroxide in 1:1 v/v of methanol/water incubated for three hours [30]. After completion of the synthesis, the peptide was cleaved from the resin and was purified by reverse-phase liquid chromatography. The

obtained peptides were identified by MALDI-TOF-MS. Cy7-modified peptides were synthesized by modifying sulfo-Cy7-NHS on the N-terminus of peptide **1** and **2** in DFM.

Preparation of HSA/ANS complex

In order to calculate the binding affinity of ANS to HSA, first, titration of 2 μM ANS was conducted with different concentrations of HSA to reach the saturation of ANS fluoerscence intensity. Fluorescence intensity of ANS versus the concentration of HSA is plotted in the Figure 3.8. For higher HSA concentrations of Figure 3.8, double reciprocal plot of the fluorescence intensity (FI) versus HSA concentration was plotted (Figure 3.9). Normalized fluorescence intensity (FI_{nor}) or the molar fluorescence intensity of bound ANS to HSA was defined as

$$FI_{nor} = 1/\text{Y intercept value}/[\text{ANS}]$$

On the other hand, an HSA solution of 2 μM was titrated with different concentrations of ANS and obtained fluorescence intensity is plotted in Figure 3.10. As it can be seen in the Figure 3.10, at a concentration of about 15 μM, fluorescence intensity becomes saturated and constant. Therefore, a concentration ratio of 1:7.5 μM [HSA]:[ANS], was decided for preparation of the HSA solution saturated with bound ANS (HSA/ANS complex).

The ANS concentration bound to HSA and the free ANS concentration were indicated as

$$[\text{ANS}]_{\text{bound}} = \frac{FI}{FI_{\text{nor}}}$$

$$[\text{ANS}]_{\text{free}} = [\text{ANS}] - [\text{ANS}]_{\text{bound}}$$

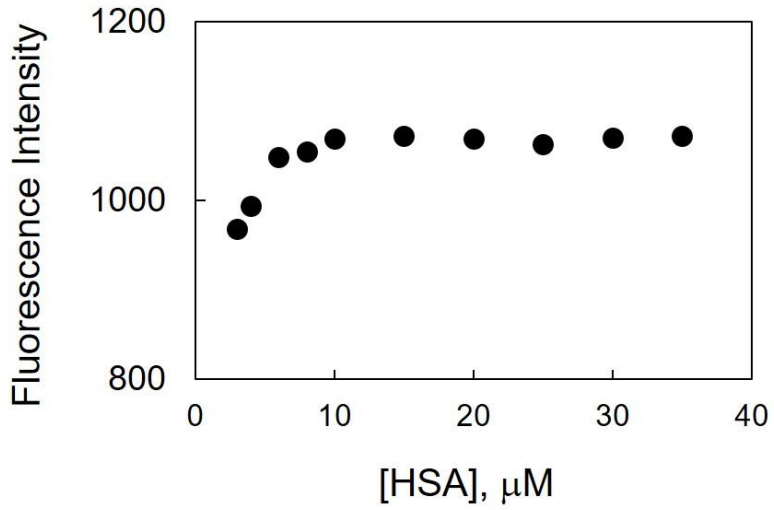

Figure 3.8. Plotting of the fluorescence intensity of ANS versus concentration of HSA.

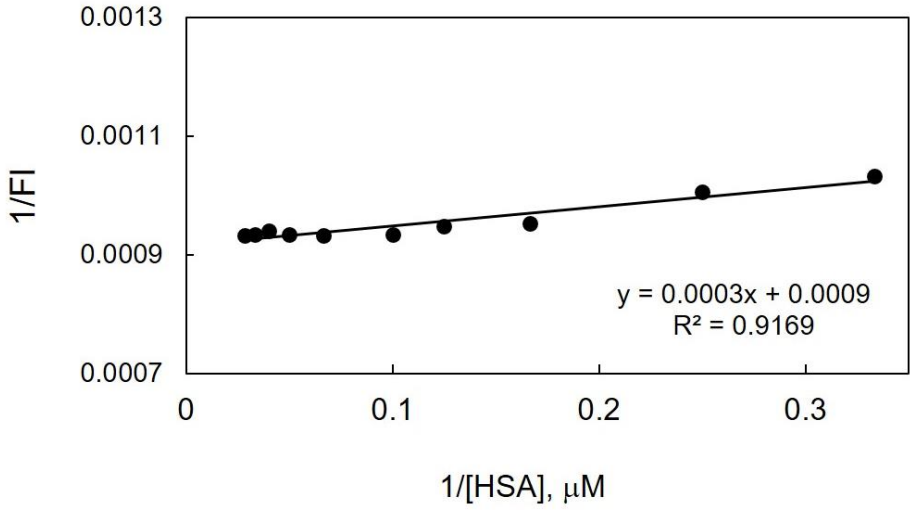

Figure 3.9. Double reciprocal plot of the fluorescence intensity of ANS versus HSA concentration.

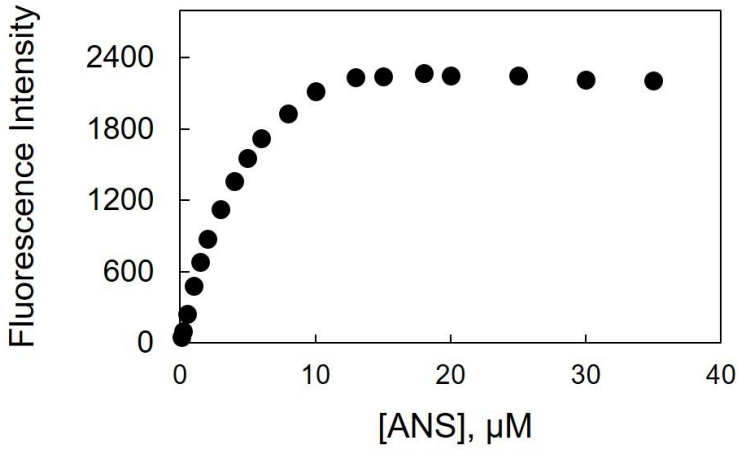

Figure 3.10. Titration of 2 μM HSA solution with ANS.

Fluorescence titrations

Stock solutions of 40 μM HSA and 100 μM ANS were prepared by dissolving HSA and ANS•Na, respectively, into 10 mM sodium phosphate buffer (pH 7.4). The HSA solution saturated with bound ANS (HSA/ANS complex) was prepared by mixing the HSA and ANS solutions with their final concentration ratio of 1.0 and 7.5 μM, respectively, followed by incubation at 25°C for an overnight for equilibration. The molar fluorescence intensity of the ANS bound to HSA was obtained by titration of ANS with HSA by changing the HSA concentration while maintaining the ANS concentration constant at 2 μM. To examine the binding affinity of ligands (the synthesized peptides and myristic acid) to HSA and their effect on the replacement with the bound ANS, 2.97 ml of HSA/ANS solution was titrated with 0.03 ml of ligand solutions with different concentrations. Sample solutions were mixed in a 1-cm path length fluorescence cell and let for equilibration for about 10 minutes at 25°C before the measurement. The fluorescence intensity of ANS was measured with an excitation and emission wavelength of 373 and 466 nm, respectively. The decrease of the fluorescence intensity caused by the addition of the ligands was extrapolated as the measure of the displacement of the bound ANS to HSA with the ligands.

Animal experiment

Animal studies were performed in accordance with the Guidelines for Animal Care and Use Committee at Kyushu University (Fukuoka, Japan). Five-week-old ICR female mice (ca. 25 g) were injected intravenously through the tail with 2.1 nmol of **1**-Cy7 and **2**-Cy7 in PBS. At 6 h after injection, mice blood was collected in heparinized tubes by cardiac puncture under anesthesia. Plasma was obtained centrifuging the blood samples at 1200 x g for 10 min at 4°C. Fluorescence intensities of the retained peptides in the plasma were measured. Results are expressed as mean ± SD (n = 4).

3.5 References

[1] J. Milton Harris and R. B. Chess, *Nat. Rev. Drug Discov.*, 2003, **2**, 214–221.

[2] Y. S. Youn, S. Y. Chae, S. Lee, J. E. Jeon, H. G. Shin and K. C. Lee, *Biochem. Pharmacol.*, 2007, **73**, 84–93.

[3] P. Milla; F. Dosio; L. Cattel, *Curr. Drug Metab.*, 2012, **13**, 105–119.

[4] T. Ishida and H. Kiwada, *Int. J. Pharm.*, 2008, **354**, 56–62.

[5] J. T. Sockolosky, S. Kivimäe and F. C. Szoka, *PLoS One*, 2014, **9**, 1–10.

[6] B. Wu and Y. N. Sun, *J. Pharm. Sci.*, 2014, **103**, 53–64.

[7] R. E. Kontermann, *Curr. Opin. Biotechnol.*, 2011, **22**, 868–876.

[8] J. T. Andersen and I. Sandlie, *Drug Metab. Pharmacokinet.*, 2009, **24**, 318–332.

[9] D. Sleep, J. Cameron and L. R. Evans, *Biochim. Biophys. Acta*, 2013, **1830**, 5526-5534.

[10] B. Elsadek and F. Kratz, *J. Control. Release*, 2012, **157**, 4–28.

[11] M. T. Larsen, M. Kuhlmann, M. L. Hvam and K. A. Howard, *Mol. Cell. Ther.*, 2016, 1–12.

[12] D. Xie, C. Yao, L. Wang, W. Min, J. Xu, J. Xiao, M. Huang, B. Chen, B. Liu, X. Li and H. Jiang, *Antimicrob. Agents Chemother.*, 2010, **54**, 191–196.

[13] S. Curry, P. Brick and N. P. Franks, *Biochim Biophys Acta.*, 1999, **1441**, 131–140.

[14] J. R. Simard, P. A. Zunszain, J. A. Hamilton and S. Curry, *J. Mol. Biol.*, 2006, **361**, 336–351.

[15] S. Curry, H. Mandelkow, P. Brick and N. Franks, *Nat Struct Biol.*, 1998, **5**, 827–835.

[16] P. Kurtzhals, S. Havelund, I. Jonassen, B. Kiehr, U. D. Larsen, U. Ribel and J. Markussen, *Biochem. J.*, 1995, **312**, 725–731.

[17] S. Havelund, A. Plum, U. Ribel, I. Jonassen, A. Vølund, J. Markussen and P. Kurtzhals, *Pharm. Res.*, 2004, **21**, 1498–1504.

[18] H. E. H. Arder and L. E. N. E. N. Ielsen, *Diabetes Care*, 2004, **27**, 1915-1921

[19] Z. J. Yasseen, *J. Biomed. Sci*., 2016, **5**, 1–8.

[20] D. Matulis, C. G. Baumann, V. a Bloomfield and R. E. Lovrien, *Biopolymers*, 1999, **49**, 451–458.

[21] K. Takehara, K. Yuki, M. Shirasawa, S. Yamasaki and S. Yamada, *Anal. Sci.*, 2009, **25**, 115–120.

[22] H. T. Akiguchi, S. A. Sanuma, J. K. Amiyama, H. M. Urata, Y. H. Asegawa, S. Y. Oshizawa, H. H. Otta, T. O. Dake, T. U. Memura, K. S. Ato and K. T. Sunoda, *Anal. Sci.*, 2017, **33**, 22–25.

[23] L. a Bagatolli, S. C. Kivatinitz, F. Aguilar, M. a Soto, P. Sotomayor and G. D. Fidelio, *J. Fluoresc.*, 1996, **6**, 33–40.

[24] X. M. He and D. C. Carter, *Nature*, 1992, **358**, 209–215.

[25] J. F. K. James Andrew Goodrich, *Binding and kinetics for molecular biologists*, Cold Spring Harbor Laboratory Press, Cold Spring Harbor, New York, 2007, 33-36

[26] K. Takehara, Y. Morinaga, S. Nakashima, S. Matsuoka, H. Kamaya and I. Ueda, *Anal. Sci.*, 2006, **22**, 1571–1575.

[27] Y. Fang, G. C. Tong and G. E. Means, *Biochim. Biophys. Acta*, 2006, **1764**, 285–91.

[28] D. I. Cattoni, S. B. Kaufman and F. L. G. Flecha, *Biochim. Biophys. Acta.*, 2009, **1794**, 1700–1708.

[29] T. Kosa, T. Maruyama and M. Otagiri, *Pharm. Res.*, 1997, **14**, 1607–1612.

[30] T. Conroy, K. A. Jolliffe and R. J. Payne, *Org. Biomol. Chem.*, 2009, **11**, 2255-2258.

CHAPTER 4

Conclusions

Thanks to the particular molecular and biological characteristics that the human serum albumin (HSA) has, developing strategies to design HSA-based drugs have been extensively evolved. Whether conjugation of these drugs with HSA is through non-covalent, covalent or genetic engineering, the ultimate purpose is to enhance the pharmacokinetic profile of the compound. HSA is the major circulating protein in the blood which has a long half-life of about three weeks. HSA also has a great ability to carry various types of endogenous and exogenous compounds in the blood, including different drugs. Thereby, affecting their distribution, absorption, metabolism and excretion profile. In a vast variety of disorders such as tumor tissues and inflamed sites. On the other hand, among the therapeutic compounds, proteins and peptides are very promising due to their selectivity, efficacy, and safety. However, their rapid elimination by enzymatic degradation or renal clearance has hindered their usage. To address this issue and to utilize the benefits of HSA, development of a more general and simpler delivery system based on HSA is required. In this thesis, I approached this goal through two methods.

In chapter 2, I could successfully enhance the blood circulation ability of a small fluorescent probe by modification of a palmitoyl group on a folate-fluorophore conjugate in mice model. The alkylated probe maintained its specificity for binding to folate receptors which are overexpressed in many cancer cell types. Meanwhile, it induced an extended blood circulation through non-covalent binding to mouse serum albumin, compared with the probe lacking the alkyl group. It is supposed that this modified alkyl group could make non-covalent binding to the hydrophobic pockets of albumin. As a result, retaining the fluorescent probe for an extended time in the blood and higher accumulation in the tumor region. This result can be promising for the development of small fluorescent probes in near-infrared imaging used in the intraoperative imaging.

In chapter 3, I reported a novel design of peptide-based ligand with a strong binding affinity to human serum albumin (HSA), which can be used as a tag to extend the blood circulation of the small size molecules. I designed these ligands with dual alkyl groups connected with a negatively charged spacer. By a competitive binding technique, it was found out that the designed dual alkylated peptides with the tuned and shorter spacer were able to

specifically share the HSA's binding pockets 4 and 6 for fatty acids, with a significantly higher binding affinity than that of the single alkylated peptide. Additionally, Cy7 modified dual alkylated peptide showed higher retention in the mice blood circulation than that of a single alkylated peptide, suggesting higher binding affinity of the former type of peptide to mouse serum albumin. No crystal structure of mouse serum albumin has so far been reported. But based on amino acid sequential studies, essential residues for the binding of fatty acids are nearly entirely conserved among all species. Thus, a similar binding behavior from human serum albumin and mouse serum albumin is expected.

The novel approaches and findings in this research, may provide new insights into the development of more straightforward methods to utilize the unique advantages of HSA. And in a broader sense, they can lead realizing of more efficient and cheaper medications for severe diseases.

Achievements

List of publications

1. **Elnaz Nakhaei**, Chan Woo Kim, Daiki Funamoto, Hikari Sato, Yuta Nakamura, Akihiro Kishimura, Takeshi Mori and Yoshiki Katayama, "Design of a ligand for cancer imaging with long blood circulation and an enhanced accumulation ability in tumors", *Journal of MedChemComm* 2017, 8, 1190-1195, [selected as Hot Article]

2. **Elnaz Nakhaei**, Ko Takehara, Hikari Sato, Khadijah Zai, Akihiro Kishimura, Takeshi Mori and Yoshiki Katayama, "A Dual Alkylated Peptide-ligand Enhances Affinity to Human Serum Albumin", *Journal of Analytical Sciences*, in press.

List of supplementary publications

1. Hikari Sato, Yuta Nakamura, **Elnaz Nakhaei**, Daiki Funamoto, Chan Woo Kim, Tatsuhiro Yamamoto, Akihiro Kishimura, Takeshi Mori and Yoshiki Katayama, "A liposome reversibly coated with serum albumin", *Journal of Chemistry Letters* **2014**, 43, 1481-1483

2. Daiki Funamoto, Daisuke Asai, Kazuki Sato, Yoko Yamaguchi, Chan Woo Kim, Hikari Sato, **Elnaz Nakhaei**, Shino Matsumoto, Takuma Yoshikawa, Koichi Sasaki, Tatsuhiro Yamamoto, Akihiro Kishimura, Takeshi Mori and Yoshiki Katayama, "Antibody Internalization into Living Cells via Crosslinker-mediated Endocytosis", *Journal of Chemistry Letters*, **2015**, 44, 468-470

List of presentations

1. “Serum albumin-mediated delivery of a fluorescent molecular probe for tumor imaging”, Poster presentation in 63rd SPSJ (The Society of Polymer Science, Japan) international annual meeting, Nagoya, Japan, May 28-30, 2014
2. “A novel tumor imaging fluorescent probe delivered through the mediation of human serum albumin”, Poster presentation in Japan Chemical Analysis Symposium, Kyushu Young Researchers, Kitakyushu, Japan, July 25-26, 2014
3. “Enhancement of blood circulation of tumor imaging fluorescent probe by human serum albumin mediation”, Poster presentation in the 2015 International Chemical Congress of Pacific Basin Societies, Honolulu, Hawaii, USA, December 15-20, 2015

Acknowledgments

Completion of this research work and dissertation could not be achieved without the assistance, cooperation and understanding of multiple people.

First and foremost, I want to express my sincere gratitude to my supervisor Professor Yoshiki Katayama for his sustained support during the five years and a half of my student life in his laboratory. Under his guidance and advisory I was able to tackle the hurdles that I was facing during my experimental and research path. To me, his constant understanding and back up was always the greatest motivation to be able to keep doing my best and going forward.

Special mention goes to my research advisor, Associate Professor Takeshi Mori. He patiently and generously devoted his time helping me who came from a different academic background, to have a better understanding of biochemical disciplines and the related experiments. His valuable advice on my study became the foundation of the success of my work. I am thankful to him as he patiently taught me the correct way of making advanced presentations or writing decent scientific papers, which were accompanied with reminding me many subtle yet important points.

I would like to express my sincere thanks to Associate Professor Akihiro Kishimura for his valuable advice on my experimental procedures during discussions and presentations.

I am deeply grateful for the collaborative assistance of Associate Professor Ko Takehara. He generously provided me with his methodological knowledge and findings of HSA/ANS titration assay, which was a critical part in my research hypothesis.

In the beginning of my immature research path I received several kind help and advice from Dr. Chan Woo Kim, Dr. Daiki Funamoto and Mr. Satoshi Kushio in peptide synthesis, purification and in vitro experiments, which I greatly appreciate them. I would also like to express my special thanks to my research fellows, Hikari Sato and Takanobu Nobori for the discussion times that we had over my research ideas and their assistance with my Japanese language. Also, I would like to appreciate the generous helps of Khadijah Zai in animal experiments and her valuable suggestions.

My sincere thanks to all my doctoral thesis committee members, Professor Masahiro Goto and Associate Professor Hiroshi Mizumoto, for their time and invaluable advice on my thesis project.

My fruitful educational stay in the prestigious Kyushu University and Katayama laboratory could not be realized without the financial support from the Ministry of Education, Culture, Sports, Science and Technology (MEXT), which I am greatly appreciative.

Finally, but by no means least, thanks go to my beloved mother and brother for their compassionate support throughout my study in abroad.

Elnaz Nakhaei
Kyushu University
March 2018